Transcriptomic similarities and differences between mouse models and human Alzheimer's Disease

Marco Antônio De Bastiani[1]*, Bruna Bellaver[1]*, Giovanna Carello-Collar[1], Maria Zimmermann[2,3], Peter Kunach[2,3,4], Ricardo A. S. Lima-Filho[5], Stefania Forner[6], Alessandra Cadete Martini[7], Tharick A. Pascoal[8], Mychael V. Lourenco[5], Pedro Rosa-Neto[2,3,4], Eduardo R. Zimmer[1,9,10]

[1]Graduate Program in Biological Sciences: Biochemistry, Universidade Federal do Rio Grande do Sul (UFRGS), Porto Alegre, Brazil

[2]Department of Neurology and Neurosurgery, Montréal Neurological Institute, McGill University, Montréal, Québec, Canada

[3]Translational Neuroimaging Laboratory, Douglas Research Institute, McGill University, Montréal, Québec, Canada

[4]Douglas Hospital Research Centre, Montreal, Canada

[5]Institute of Medical Biochemistry Leopoldo de Meis, Federal University of Rio de Janeiro, 21941-902, Rio de Janeiro, RJ, Brazil

[6]Institute for Memory Impairments and Neurological Disorders (UCI MIND), University of California, Irvine, USA

[7]Department of Pathology & Laboratory Medicine, University of California, Irvine, USA

[8]Department of Psychiatry, University of Pittsburgh School of Medicine, Pittsburgh, PA, USA

[9]Department of Pharmacology, UFRGS, Porto Alegre, Brazil

[10]Graduate Program in Biological Sciences: Pharmacology and Therapeutics, UFRGS, Porto Alegre, Brazil.

*These authors contributed equally to the article.

Corresponding author:
Eduardo R. Zimmer, PhD (E.R. Zimmer)
Department of Pharmacology, Universidade Federal do Rio Grande do Sul (UFRGS)
2500 Ramiro Barcelos street, 90035-003, Porto Alegre, RS, Brazil
Email address: eduardo.zimmer@ufrgs.br
Telephone: +55 51 33085558
Fax: +55 51 33085544
Website: www.zimmer-lab.org

Abstract

Alzheimer's disease (AD) is a multifactorial pathology, with most cases having a sporadic origin. Yet, preclinical research studies relied for decades on transgenic models overexpressing human genes found in autosomal dominant familial AD patients. Recently, knock-in (KI) models have been developed with the promise of resembling better sporadic human AD, such as the novel hAβ-KI mouse. However, their phenotypes and translational power are still being addressed. To unveil core molecular programs in AD, we compared hippocampal transcriptomic profiles of transgenic (5xFAD and APP/PS1) and KI (hAβ-KI) mouse models with early- (EOAD) and late- (LOAD) onset AD patients. A comparison of differential expression analyses showed seven genes (S100A6, C1QB, CD33, CD14, SLC11A1, KCNK1, and SST) consistently altered among models and human AD. Experimental validation of these genes revealed four altered in mice (SLC11A1, S100A6, CD14, CD33, C1QB) and three in humans (S100A6, SLC11A1, KCNK). Surprisingly, our analysis unveiled that the three mouse models, including the gene overexpression models, presented more Gene Ontology biological processes (GOBP) terms and enriched signaling pathways in common with LOAD than with EOAD individuals. Furthermore, the semantic similarity of enriched GOBP terms highlighted model-specific biological alterations that deserve further attention. Finally, we identified 17 transcription factors potentially acting as master regulators of AD. Our cross-species analyses revealed that the three mouse models presented a remarkable similarity to LOAD, with the hAβ-KI being more specific for LOAD. However, the representation of biological processes altered in each model may differ. Our findings suggest that if selected according to molecular and cellular mechanisms aimed for investigation, the currently available models are helpful tools for advancing our understanding of AD.

Keywords: Alzheimer’s disease mouse models; humanized Aβ knock-in; APP/PS1; 5xFAD; bioinformatics.

Introduction

Alzheimer's disease (AD) is commonly categorized into early- (EOAD; <65 years old) and late-onset (LOAD; ≥65 years old) based on the age of clinical onset, the latter being the most prevalent form of the disease[1]. This broad definition includes the mendelian and non-mendelian EOAD, which confers an additional degree of heterogeneity to this group. Both forms of EOAD seem to present more prominent brain atrophy, glucose hypometabolism and increased tau PET uptake compared to LOAD[2–6]. However, a recent study demonstrated a similar biomarker profile between autosomal dominant EOAD and LOAD patients, supporting a shared pathobiological construct between both forms of the disease[7].

Autosomal dominant inheritance mendelian EOAD accounts for less than 10% of the cases, but gene mutations found in these patients have been used for developing most AD models[1]. More specifically, mouse models overexpressing one or more mutations in the amyloid precursor protein (APP), presenilin 1 (PSEN1), and presenilin 2 (PSEN2) have dominated the AD experimental research. However, these models have undergone extensive scrutiny in the past years because these overexpression models present artifacts introduced by APP overexpression and do not resemble important aspects of LOAD[8,9,10]. Thus, a major challenge in the field has been the development of animal models that better recapitulate LOAD. The emergence of a new knock-in (KI) strategy for developing novel models expressing human APP with appropriate levels and cellular specificity seems to provide improved models for investigating sporadic AD[10–12].

The investigation of core molecular programs shared by overexpression and KI models with human pathology may help determine to what extent animal models can resemble human disease. Additionally, the ability to recapitulate key molecular pathways activated or repressed in AD is crucial for model validity. Here, we aimed to ascertain the genes and pathways overlapping gene overexpression (5xFAD and APP/PS1) and KI (hAβ-KI) mouse models with EOAD and LOAD. With this in mind, we compared the hippocampal transcriptomic profiles of these animal models and AD and established the molecular similarity

and specificity of mouse data to the human disease. We further employed a regulatory network-based approach to infer and investigate common master regulators between animal models and AD. Finally, we validated our transcriptomic exploratory findings in the hippocampus of APP/PS1 mice and *post-mortem* EOAD and LOAD individuals.

Results

hAβ-KI, 5xFAD, and APP/PS1 models exhibit more differentially expressed genes overlapping with LOAD than EOAD

Differential expression analysis of the hippocampus of hAβ-KI, 5xFAD, and APP/PS1 mice and their wild type (WT) controls identified 1537, 3231, and 1768 differentially expressed genes (DEGs), respectively (unadjusted p-value < 0.05; **Figure 1A, B; Supplemental Figure S1, Supplemental Table 2**). We found that the hAβ-KI animals presented more DEGs overlapping with the 5xFAD mice than with APP/PS1 model [389 (25.3%) *versus* 235 (15.3%) DEGs, respectively; Chi-square adjusted p-value < 0.001; **Figure 1C**]. In addition, the comparison with AD human data demonstrated that hAβ-KI mice exhibited more DEGs in common with LOAD than with EOAD individuals (381 *versus* 164, respectively; **Figure 1D, E**). Despite being mouse models carrying familial AD-linked mutations, APP/PS1 and 5xFAD mice shared more DEGs with LOAD than with EOAD patients (**Figure 1D, E**). Moreover, considering the total of DEGs identified in the mouse models as reference (model-disease overlap), the intersection of DEGs between 5xFAD and EOAD was significantly higher (14%) than the overlap between both APP/PS1 (10.9%; Chi-square adjusted p-value = 0.0061) or hAβ-KI (10.7%; Chi-square adjusted p-value = 0.0054) with EOAD (**Figure 1D - right**). On the other hand, the overlap of LOAD DEGs with 5xFAD (28%) and with APP/PS1 (25.3%) mice was not significantly different from the overlap with hAβ-KI (24.8%; **Figure 1E - right**; Chi-square adjusted p-value = 0.123 and Chi-square adjusted p-value = 0.063, respectively). Interestingly, the hAβ-KI model shared 212 DEGs exclusively with LOAD, while only 98 with EOAD (**Figure 1A, B**). When we compared only the adjusted p-value DEGs [Benjamini &

Hochberg (BH) > 0.1] we observed a similar profile/proportion of gene overlap, especially regarding the hAβ-KI model and LOAD (**Supplemental Figure S2**). Thus, we opted for using unadjusted p-values < 0.05 for subsequent functional enrichment analysis, which allows for exploratory cross-species analysis of core molecular programs that can be further validated. Only seven DEGs were found in common with all the mouse models and human AD. Among them, DEGs related to innate immune response (C1QB, CD33, CD14, and SLC11A1) were consistently upregulated across the groups, while those related to membrane potential regulation and neuropeptide production (KCNK1 and SST) were mostly downregulated. The S100A6 gene, found in neurons and some populations of astrocytes, was upregulated in all conditions (**Supplemental Table 2**).

The protein-protein interaction (PPI) network revealed that PTGES3, GNB1, ARIH2, SMURF1, EIF3A genes are hubs of the four clusters formed (**Figure 1F**). However, only two genes revealed in the PPI network – GNB1 and NKTR – were differentially expressed in the hAβ-KI model after BH adjustment. Considering the DEGs exclusively shared with the hAβ-KI model and EOAD patients, only 11 remained in the PPI network, and only the PRPF40A gene remained significant in hAβ-KI after multiple comparisons correction (**Figure 1G**). Next, we compared the DEGs of each mouse model with a database from multiple sclerosis (MS) patients to verify the specificity of these models for AD pathology. The three mouse models presented a greater overlap of DEGs with AD than with MS individuals (**Figure 1H, I; Supplemental Figure S3A, B**). Interestingly, no significant differences were observed in DEGs shared between hAβ-KI mice and EOAD (10.7%) or MS patients (9.6%; **Figure 1J; Supplemental Figure S3C**), while the overlap of hAβ-KI DEGs with LOAD was significantly higher than with both EOAD and MS (24.8%; Chi-square adjusted p-value < 0.001; **Figure 1J**; **Supplemental Figure S3C**).

To validate our exploratory transcriptomic findings, we performed qRT-PCR analyses of the seven DEGs overlapping between human AD and animal models. The validation was performed in APP/PS1, LOAD, and EOAD *post-mortem* hippocampus. Significant

increases in of S100A6, C1QB, CD33, CD14, and SLC11A1 mRNA levels were observed in APP/PS1 mice compared to WT littermates (**Figure 2A**). Regarding the human hippocampal tissue validation, S100A6 was significantly increased in LOAD and EOAD compared to cognitively unimpaired (CU) individuals (**Figure 2B**). In addition, SLC11A1 expression increased, while KCNK significantly decreased in LOAD individuals. Although the other genes presented decrease/increase trends in AD patients compared to CU individuals, they did not reach statistical significance.

hAβ-KI mice and LOAD patients present higher similarities in functional changes

Functional enrichment analysis of gene ontology for biological processes (GOBPs) revealed that ~ 92% of the GOBPs enriched in hAβ-KI mice overlap with enriched terms in LOAD patients (**Figure 3B, E - right**) in the model-disease approach, while the intersection with EOAD was markedly low (around 32%, **Figure 3A, D - right**). The remaining 8% of GOBP terms not shared between hAβ-KI mice and LOAD were related to RNA splicing and protein phosphorylation (**Supplemental Table 3**). Additionally, the hAβ-KI mice presented a higher number of enriched GOBP terms in joint with 5xFAD (79.2%) than with APP/PS1 (56.1%) model (**Figure 3C**; Chi-square adjusted p-value < 0.001). Surprisingly, 5xFAD and APP/PS1 shared more than 75% of their enriched GOBPs with LOAD patients (**Figure 3B, E - right**) and only ~ 45% with EOAD (**Figure 3A, D - right**). However, we observed that about 50% of GOBPs overlap between EOAD, LOAD and 5xFAD, indicating a lack of disease subtype specificity for this model (**Supplemental Table 3**). The comparison among the GOBPs of the three models with MS demonstrated, however, greater specificity of these mouse models for AD (**Supplemental Figure S3)**. **Figure 3F-H** shows that all mouse models evaluated presented less than 5% of enriched GOBP terms in common with MS.

hAβ-KI mice present less GOBP terms intersection with EOAD patients compared to APP/PS1 and 5xFAD mice

The union of enriched GOBP intersecting terms in the mouse models and human AD was generated to better visualize the common biological processes altered in each group. "Regulation of cytokine secretion" (13 nodes), "regulation of catabolic processes" (3 nodes), "NFκB signaling" (9 nodes), and "intracellular transport and secretion" (21 nodes) were among the GOBP terms enriched in the hippocampus of the three mouse models and EOAD patients (**Figure 4**; light gray circles). These terms are mainly related to cellular response to stressor agents, hormones and cytokines, immune response, and calcium homeostasis and transport. Interestingly, GOBP terms related to oxidative phosphorylation found in EOAD are only enriched in the APP/PS1 model (purple circles).

hAβ-KI mice and LOAD patients exhibit greater overlap among the enriched GOBP terms

Figure 5 shows that hAβ-KI mice GOBP terms are more represented among the GOBPs in common with LOAD (**yellow, purple, and pink circles**) than with EOAD. “PI3K and NFkB signaling pathways” (20 nodes), “regulation of neuronal development” (19 nodes), “regulation of neurotransmitter and hormone secretion” (31 nodes), “regulation of immune response” (22 nodes), “antigen processing and presentation” (21 nodes) and “phospholipid and ribose phosphate metabolism” (10 nodes) are among the enriched biological processes shared between all three mouse models and LOAD (**pink circles**). Interestingly, “glucose, cholesterol and purine metabolism”, “regulation of MAPK cascade”, and “calcium homeostasis” only appeared enriched in 5xFAD and APP/PS1 mice (**gray circles**).

Most of the hAβ-KI enriched KEGGs are shared with LOAD patients

The most affected pathways related to changes in transcriptome profile were identified using enrichment analysis of KEGG canonical pathways. **Figure 6A, B** shows that among the 10 KEGGs found significantly enriched in the hAβ-KI model, six were also

identified in LOAD patients ["glutamatergic and GABAergic synapse" (adjusted p-value = 0.017), "calcium signaling" (adjusted p-value = 0.040), "Rap1 (adjusted p-value = 0.040) and Ras signaling (adjusted p-value = 0.040)" and "choline metabolism in cancer" (adjusted p-value = 0.041)], while only one was enriched in EOAD patients ["amyotrophic lateral sclerosis" (adjusted p-value = 0.040); **Supplemental Table 4**]. KEGG analysis also revealed that APP/PS1 was the mouse model that presented the highest percentage of pathway overlap with EOAD (36.7%; **Figure 6C**) and LOAD (73.3%; **Figure 6D**). Interestingly, most of the intersection between APP/PS1 and human AD is represented by KEGGs related to other neurodegenerative diseases (e.g. Parkinson's disease, Huntington's disease) or bacterial infection (e.g. *Escherichia coli*, *Salmonella* spp.; **Supplemental Table 4**). Despite PI3K pathway-related GOBPs appearing enriched in LOAD, they were only significantly altered in the hAβ-KI model (adjusted p-value = 0.040) in the KEGG analysis. "Rap1 and Ras signaling pathways" and "adhesion and apoptosis" were found consistently altered in the APP/PS1 and hAβ-KI models (**Figure 6H, I; Supplemental Table 4**). In addition, the 5xFAD was the mouse model that presented more enriched KEGG terms (**Figure 6G; Supplemental Table 4**). Similar to the GOBP enrichment analysis, 5xFAD presented more pathways shared with LOAD (56.9%) than with EOAD (13.8%; **Figure 6C, D**), which were mainly related to synaptic neurotransmission and insulin regulation (**Supplemental Table 4**). Additionally, alterations in apoptosis- and endocannabinoid system-related pathways were observed in the 5xFAD model and the human disease (**Supplemental Table 4**). Despite an overlap in KEGGs associated with inflammatory diseases and bacterial infections between 5xFAD and AD, well-studied signaling pathways in the context of inflammation were only observed in the 5xFAD model (e.g., TNF, Toll-like, NFκB).

EOAD and LOAD patients share two enriched master regulators with overexpressing and knock-in AD mouse models

To identify elements located in higher positions of the biological system hierarchy, we performed a master regulator analysis to determine transcription factors

potentially driving the biological alterations observed in AD. In addition, we asked if these elements were also orchestrating the transcriptional profile changes in mouse models. Our analysis revealed a total of 95 master regulators enriched within DEGs emerging in at least one experimental group (**Figure 7A, B; Supplemental Table 5**). Interestingly, both 5xFAD and APP/PS1 mouse models presented more master regulators in common with LOAD than with EOAD, while hAβ-KI mice exhibited a similar overlap with both subtypes of human AD (**Figure 7A, B**). Among the 17 master regulators identified in ≥ 4 groups, only PARK2 and SOX9 were enriched in the three models and in the human disease (**Figure 7C**). Next, two-tail gene set enrichment analysis (GSEA) was performed to infer the activation state of each candidate. We observed that, while PARK2 is repressed, SOX9 is activated across the disease/animal model phenotypes evaluated (**Figure 7D**). In addition, FOXC2 and ZNF461 were identified exclusively in the hAβ-KI mice and LOAD individuals (**Supplemental Table 5)**. The three mouse models share eight enriched master regulators, most of which involved in regulating cell cycle and apoptosis (**Supplemental Table 5**). A second methodological approach to infer activation of transcription factors was also applied, and similar results were observed for the 17 master regulators candidates (**Supplemental Figure S4**). Finally, a comparison with a previously published study that investigated master regulators associated with AD showed that 11 out of 17 MR identified here were also enriched in that dataset (**Figure 7E**).

Discussion

In the past years, significant efforts of collaborative initiatives generated multiple mouse models with the promise of better recapitulating the phenotypic spectrum of sporadic LOAD. The evaluation of these animal models' phenotype is a work in progress. Here, we evaluated hippocampal similarities and differences of three mouse models (APP/PS1, 5xFAD, and the novel hAβ-KI) at the transcriptional level. An exploratory cross-species comparative transcriptomics was also conducted to evaluate shared molecular core programs between these models and EOAD/LOAD cases. All mouse models showed more similarities to LOAD than to

EOAD patients. The hAβ-KI mouse model presented not only a remarkable transcriptomic similarity for LOAD but also a specificity, and, surprisingly, the gene overexpressing models also better resemble LOAD than EOAD.

The specificity of the hAβ-KI model for LOAD was first observed in the exploratory DEG analysis, as hAβ-KI mice presented twice more DEGs exclusively overlapping with LOAD than with EOAD patients. Further PPI network analysis of these DEGs identified gene products that interact with each other to accomplish different biological functions. For example, we found clusters involved in ribosomal RNA processing, inflammatory response, and E3-ubiquitin ligase-related immune response, all phenomena well described in AD[13–15]. In line with this, Baglietto-Vargas and colleagues recently demonstrated that hAβ-KI mice presented a decreased production of the anti-inflammatory cytokines IL-2 and IL-10 compared to age-matched WT animals[11]. Importantly, a cluster of genes encoding G protein and G protein-coupled receptors (GPCRs) was also evidenced in our study. G proteins act as modulators or transducers in various transmembrane signaling systems, and GPCRs are implicated in multiple stages of AD pathogenesis[16]. Specifically, the glycogen synthase kinase 3-β (GSK3-β) was identified as a major tau kinase, mediating tau phosphorylation and, consequently, being an active player in the development of tau pathology in AD[17]. Interestingly, this process seems to depend on the PI3K signaling activation[18], a pathway significantly altered in the hAβ-KI mice. The clusters identified with our network analysis might shed light on the understanding of pathogenic mechanisms of LOAD that can be recapitulated by the novel hAβ-KI mouse model, facilitating the search for therapeutic targets. Importantly, network-based approaches have already proven to be a powerful strategy to identify elements, pathways, or functional modules in several other brain diseases[19,20] compared to evaluating single genes.

Interestingly, only seven (C1QB, CD33, CD14, SLC11A1, KCNK1 and SST) out of 7868 DEGs identified in our transcriptomics analysis were shared among the mouse models, EOAD and LOAD patients. Multiple studies have already implicated these genes in AD pathophysiology. For instance, a decrease in somatostatin (SST) gene expression in AD brains

has been previously reported[21]. Interestingly, SST was shown to be the most selectively enriched binder to soluble oligomeric Aβ in the human brain, influencing Aβ aggregation and masking the ability of widely-used antibodies to detect Aβ[22]. Nilsson and colleagues further demonstrated that modulation of the SST receptors Sst1 and Sst4 regulates neprilysin, the major Aβ-degrading enzyme[23]. The consistent findings observed in our study suggest that SST role in AD pathology seems to be conserved cross-species. Additionally, we found that C1QB, CD33, CD14, and SLC11A1 genes, all associated with immune responses, were upregulated in all analyzed mouse models, as well as in EOAD and LOAD patients. Accordingly, Gjoneska and colleagues previously pointed a conserved immunological basis for AD by comparing the CK-p25 mouse model with hippocampal human *post-mortem* tissue[14]. Our qRT-PCR analysis in APP/PS1 mice confirmed alterations in these genes. The analysis in the human brain only reached statistical significance for three of the seven genes – S100A6, SLC11A1, KCNK1 – but a trend was observed for SST and C1QB. This validation step indicates that our exploratory analysis provides meaningful biological information regarding AD pathology in the hippocampus.

The identification of transcriptomic changes at the pathway level has the potential to offer insights into the biological processes disturbed in AD. Accordingly, we observed that the hAβ-KI hippocampus presented an almost complete overlap of enriched hippocampal GOBP terms with LOAD, while only about one-third was shared with EOAD. This specificity for LOAD seems to be a unique and important feature of this novel KI model, as the 5xFAD and APP/PS1 mice also presented a significant overlap with EOAD. Despite that, the scanty overlap of GOBP terms among AD mouse models and MS confirmed that these models present transcriptomic features specific to AD rather than general alterations shared among other neurodegenerative diseases. In addition, this resemblance with AD appears to be a specific feature of rodent models carrying mutated human genes related to AD-associated amyloid pathology, such as APP and PSEN1, or humanized Aβ-KI. Indeed, Burns and colleagues observed that Tg4510 mice, which express a tau mutation found in familial frontotemporal

dementia, presented the highest enrichment of genes in common with human ALS and Huntington's disease rather than with AD[24].

Impaired calcium (Ca^{2+}) handling by neurons precedes the formation of amyloid plaques and neurofibrillary tangles and has been implicated in major molecular alterations underlying AD[25]. The association between PS1 mutations and altered Ca^{2+} signaling in neurons has been known for many years[26]. Early imbalance between excitatory/inhibitory (E/I) neurotransmission, with loss of neuronal network stability, is a well-attested phenomenon in AD[27,28]. The average incidence of seizure in AD patients is around 15%, which is seven-fold higher when compared to individuals without dementia[29,30]. Aβ is able to impair the long-term potentiation, promote depression of synaptic activity and alter the brain network[28], and affect the E/I balance by impairing the inhibitory activity of the parvalbumin-expressing and SST interneurons[31,32]. Interestingly, modulation of interneuron function might improve brain rhythms and cognitive functions in AD[31,33]. Our study identified "calcium signaling" and "glutamatergic and GABAergic signaling" to be exclusively altered in the hAβ-KI mice and LOAD, pointing to this KI mouse model as an important tool to better understand calcium signaling and the E/I imbalance in AD.

Transcription factors play a key role in orchestrating phenotypic determination by regulating transcriptional targets that coordinate complex cellular processes[34,35]. Based on reverse engineering co-expression regulatory network reconstruction, we identified two transcription factors exclusively altered in the hAβ-KI model and LOAD individuals' hippocampi: ZNF461 and FOXC2. ZNF461 roles in brain function have still been poorly explored; however, this transcription factor was identified among genes that represent a polygenetic risk for psychiatric disorders, and its alteration might contribute to cortical atrophy and changes in functional connectivity[36]. On the other hand, FOXC2 function in the brain is implicated in cell proliferation and invasion in glioblastoma[37], in angiogenic processes during fetal brain development[38], and is directly regulated by cyclin-dependent kinase 5 (Cdk5) phosphorylation to control peripheral lymphatic vase development[39]. Interestingly, it has been

demonstrated that the deregulation of Cdk5 contributes to AD pathology preceding tau hyperphosphorylation and loss of synaptic proteins[40]. On the other hand, Saito and colleagues reported that the App^{NL-F} KI model did not generate p25, necessary for aberrant Cdk5 activation, suggesting that the reports about its relevance in AD might be an artifact due to the overexpression of APP in other mouse models[8]. However, several studies using organotypic hippocampal slices and primary neural cells exposed to Aβ showed increased p25 generation independently of APP overexpression[41–43], suggesting that experimental validation of FOXC2 and Cdk5 in hAβ-KI mice is needed to understand the potential link among FOXC2, Cdk5, and AD pathology.

Further, in the master regulator analysis, we identified SOX9 as a transcription factor consistently activated in the mouse models and human AD. SOX9 is a key factor in the nervous system development, especially for astrocyte and oligodendrocyte cell fate specification[44–46]. Recently, Sun and colleagues identified SOX9 as an astrocyte-specific nuclear marker in the adult human and mouse brains, presenting a remarkable expression in the murine hippocampus and cortex compared to the cerebellum[47]. However, there are no studies to date linking this transcription factor with AD, and our results highlight a promising new target for investigation in AD. In addition, PARK2 gene was also identified in the MRA as a transcription factor consistently repressed among all groups of this study. PARK2 encodes an E3 ubiquitin ligase, and its involvement in autosomal recessive parkinsonism is well established. Although less explored, its role in AD has already been demonstrated by computational[35,48] and experimental[49–51] approaches. Specifically, mitophagy failure, promoted by repression in PARK2 ability to stimulate PS1, was reported in cellular and animal models[49,51]. On the other hand, the overexpression of PARK2 promoted diminished brain accumulation of ubiquitinylated proteins, improved its targeting to mitochondria, and potentiated autophagic vesicle synthesis[50]. Our findings thus highlight the value of hAβ-KI, 5xFAD, and APP/PS1 mouse models to better understand these particularly underexplored aspects in AD.

Decades of use of animal models in AD research underline that each of them can mimic a slightly different aspect of the disease. Therefore, one could argue that animal models of AD should be selected according to the biological aspect aimed for investigation rather than be seen as a generic model. The clusterization by semantic similarity of enriched GOBP terms performed here allowed highlighted alterations specific to 5xFAD, APP/PS1 or hAβ-KI mouse models. For example, several GOBP terms associated with oxidative phosphorylation, purine metabolism, and the MAPK pathway were altered in 5xFAD and APP/PS1 mice but not in the hAβ-KI model. On the other hand, inflammatory-related processes seem to be a feature of AD pathology present in all three mouse models. Thus, the comparison of altered biological processes among mouse models and human AD presented here sheds light on the translational power of each animal model and helps to improve our mechanistic understanding of AD pathology.

Methods

Mouse Models Data Acquisition

RNA sequencing (RNA-seq) data from 5xFAD [4, 8 and 12 months-old, n = 23 hemizygous; 26 wild type (WT)] and hAβ-KI (22 months-old, n = 7 homozygous; 8 WT) AD mouse models (**Supplemental Table 1**) were obtained from AMP-AD Knowledge Portal (https://adknowledgeportal.synapse.org/) using *synapser* (version 0.7.64) and *synapserutils* (version 0.1.6) packages. Specifically, gene expression information was collected from https://www.synapse.org/#!Synapse:syn16798173 and https://www.synapse.org/#!Synapse:syn18634479 for 5xFAD and hAβ-KI models, respectively. APP/PS1 (8 and 12 months-old, n = 8 APP/PS1; 8 WT) mouse model RNA-seq data (**Supplemental Table 1**) was combined from two Gene Expression Omnibus (GEO) (https://www.ncbi.nlm.nih.gov/geo/) datasets [GSE149661[52] and GSE145907] and downloaded through NCBI Sequence Read Archive using SRAToolKit (https://github.com/ncbi/sra-tools). After quality control evaluation, the following samples were removed: sample “67-2” from hAβ-KI; samples “466”, “305”,

"456", "497" from 5xFAD. Known phenotypic features of the three mouse models evaluated in this study are depicted in **Figure 8A**.

Human Data Acquisition

Human AD hippocampal processed microarray data of five studies were obtained from GEO repository [GSE28146[53], GSE29378[54], GSE36980[55], GSE48350[56] and GSE84422[57]], downloaded using GEOquery package (v2.56.0)[58] and combined under common gene symbol annotations. Afterwards, batch correction was implemented using the sva package (v3.36.0)[59] and data was split into EOAD (age at death < 65, n = 4 EOAD; 10 cognitively unimpaired controls) and LOAD (age at death ≥ 65, n = 59 LOAD; 63 cognitively unimpaired controls) for further analyses (**Supplemental Table 1**). AD diagnosis, control definition and exclusion criteria of each GSE study are depicted in **Figure 8B**. Multiple sclerosis (n = 5 MS; 5 control) hippocampal RNA-seq data (**Supplemental Table 1**) was also obtained from GEO under the identifier GSE123496[60] and downloaded through NCBI Sequence Read Archive. Sample demographics from EOAD, LOAD and MS individuals can be found in **Figure 8C**.

RNAseq Processing

Raw data for each RNAseq dataset was downloaded and transcript alignment was performed using Salmon (v1.3.0) (Patro *et al*, 2017). Transcripts were mapped to genome using indexes derived from *Mus musculus* GRCm38 Ensembl build (ftp://ftp.ensembl.org/pub/release-96/fasta/mus_musculus) and *Homo sapiens* GRCH38 Ensembl build (ftp://ftp.ensembl.org/pub/release-96/fasta/homo_sapiens) for the mouse models and human data, respectively. Aligned reads were summarized using tximport (v1.12.3)[61] and genes with minimum mean of counts per million cut-off < 2 were filtered out.

Differential Expression Analyses

Differential expression was computed on processed microarray data using the limma package[62] *lmFit* function to fit multiple linear models by generalized least squares. In addition, *eBayes* function was used to compute moderated t-statistics, moderated F-statistic and

log-odds of differential expression by empirical Bayes moderation of the standard errors towards a common value. For RNA-seq datasets, processed expression data from each study was submitted to DESeq2 (v1.28.1)[63] method using previously created tximport Summarized Experiment. Differential expression analysis (DEA) based on the Negative Binomial distribution was computed with the *DESeq* function followed by log fold change shrinkage with the *lfcShrink* function (shrinkage estimator type = "ashr"). Genes with unadjusted p-value < 0.05 were considered as DEGs. For information about BH adjusted p-values, see **Supplemental Table 2**.

Venn diagrams for DEGs were constructed using VennDiagram package (v1.6.20)[64]. The proportion differences between overlapped genes between models and diseases were computed by Pearson's Chi−squared test with Yates' continuity correction for count data, followed by post-hoc pairwise Bonferroni adjustment.

Protein-Protein Interaction Network Reconstruction

We used the Search Tool for the Retrieval of Interacting Genes/Proteins (STRING) Consortium to build protein-protein interaction (PPI) networks. STRING is a biological database and web resource of known and predicted PPI which contains information from numerous sources, including experimental data, computational prediction methods and public text collections. The construction of the PPI networks was implemented in R using the STRINGdb (v2.0.2), RedeR (v1.36.0) and igraph (v1.2.6) packages[65–67]. For the final networks, we retained only the edges with a combined interaction score > 0.7 from all sources and highly connected nodes for the final networks.

Functional Enrichment Analyses

DEGs (unadjusted p-value < 0.05) from human or mouse model studies were submitted to Gene Ontology (GO) and Kyoto Encyclopedia of Genes and Genomes (KEGG) enrichment analysis using the clusterProfiler package (v3.16.1) *enrichKEGG* and *enrichGO* functions. The GO terms were clustered by semantic similarity using the *mgoSim* function from

GOSemSim (v2.14.2) package[68] (arguments measure = "Wang" and combine = NULL). The resulting similarity matrices were represented as GO networks using the RedeR (v1.36.0) package[65] for interactive visualization and manipulation of nested networks. Clusters of GO terms obtained from GOSemSim algorithm were manually named for their biological interpretation. Venn diagrams for enriched GO/KEGG terms were constructed using VennDiagram (v1.6.20) package. Nested networks were constructed by maintaining only the intersecting GOBP terms among the mouse models and each human pathology (either EOAD or LOAD). Finally, Jaccard coefficient > 0.7 was used to filter out edges with low gene intersection between terms. The proportion differences between overlapped terms between models and diseases were computed by Pearson's Chi−squared test with Yates' continuity correction for count data, followed by post-hoc pairwise Bonferroni adjustment.

Reverse Engineering of Transcriptional Network

The transcriptional network (TN) centered on transcription factors (TF) and their predicted target genes were inferred using a large cohort of neurologically and neuropathologically normal individuals (n = 122) obtained from GEO under the identifier GSE60862[69]. Herein, the terms “regulatory unit” or “regulon” are used to describe the groups of inferred genes and their associated TFs. RTN (v2.12.1) package was used to reconstruct and analyze TNs based on the mutual information (MI) using the Algorithm for the Reconstruction of Accurate Cellular Networks (ARACNe) method[70–72]. In summary, the regulatory structure of the network is derived by mapping significant associations between known TFs and all potential targets. To create a consensus bootstrap network, the interactions below a minimum MI threshold are eliminated by a permutation step and unstable interactions are additionally removed by bootstrap. Finally, data processing inequality algorithm is applied with null tolerance to eliminate interactions that are likely to be mediated by a third TF. The reference hippocampus TN was built using the package’s default number of 1000 permutations and 100 bootstraps (p-value < 0.001).

Master Regulators Inference and Two-Tailed Gene Set Enrichment Analysis

Master regulator analysis (MRA) was employed for the MR inference[34]. MRA computes the statistical overrepresentation of DEGs (p-value < 0.05) obtained from DEA in the regulatory units of the reference TN. The regulons were considered altered in the disease if they presented (1) statistical enrichment of DEGs, (2) regulon size > 50 and (3) ≥ 80% of the queried case-control studies. Two-tailed Gene Set Enrichment Analysis (GSEA) was also performed using the RTN package (version 2.4.6, p-value < 0.05 and 1000 permutations). Briefly, Pearson's correlation was used to split the regulatory units into positively (A) and negatively (B) associated targets. Afterwards, the phenotype association of each subgroup was tested using the GSEA[73] statistics, resulting in independent enrichment scores for each subgroup. Finally, we tested the differential enrichment (ESA – ESB) considering the following desirable criteria for clear association: (1) a maximum deviation from zero near opposite extremes and (2) a good separation of the two distributions. Thus, a high negative differential score implies that the regulon is repressed in the disorder phenotype, while a high positive one indicates that the regulon is induced.

Virtual Inference of Protein Activity by Enriched Regulon Analysis

The virtual inference of protein activity by enriched regulon analysis (VIPER) is another regulatory network-based approach to infer protein activity from gene expression profiles. Similar to MRA, VIPER systematically analyze the expression of the regulatory units previously identified by ARACNe algorithm. However, VIPER uses a fully probabilistic, yet efficient enrichment analysis framework based on analytic rank-based enrichment analysis. The analysis was implemented using the viper (v1.22.0) package in R[74].

Mice

Male and female APPSwe/PS1ΔE9 mice on a C57BL/6J (#005864) background were originally obtained from The Jackson Laboratories and bred at our animal facility. WT littermates were used as controls. All genotypes were confirmed before use and reconfirmed

after tissue extraction. Animals were housed in groups of up to five per cage with food and water *ad libitum*, under a 12 h light–dark cycle, with controlled room temperature. For qRT-PCR experiments, 14 APP/PS1 (12-16 months-old) and 16 WT mice (12-15 months-old) were used.

Human tissue

Hippocampal tissue from LOAD (n = 8, mean ± SD age = 79.5 ± 5.6, 2F/6M), EOAD (n = 7, mean ± SD age = 51.3 ± 5.6, 6F/1M) and cognitively unimpaired individuals (n = 9, mean ± SD age = 74.6 ± 8.9, 4F/5M) were obtained from the Douglas-Bell Canada Brain Bank with the approval of the scientific journal of the Brain Bank and the research ethics boards of the Douglas Institute (approval number : IUSMD20-02).

RNA extraction and qRT-PCR

Total RNA from hippocampus of LOAD, EOAD and cognitively unimpaired individuals as well as APP/PS1 and WT mice were isolated using TRIzol Reagent (Invitrogen Carlbad). The concentration and purity of the RNA were determined spectrophotometrically at a ratio of 260/280. Then, 1 µg of total RNA was reverse transcribed using Applied Biosystems™ High-Capacity cDNA Reverse Transcription Kit (Applied Biosystems, Foster City, CA), according to manufacturer's instructions. Real-time quantitative polymerase chain reaction (qRT-PCR) was performed on an Applied Biosystems 7900HT system with SYBR green master mix (Applied Biosystems). Target mRNA levels were normalized using -β actin gene (Actb) as housekeeper and cycle threshold (Ct) values were used to calculate fold changes in gene expression relatively to cognitively unimpaired individuals or WT mice using the $2^{-\Delta\Delta Ct}$. For the human RNA extraction, Direct-zolTM RNA Microprep from Zymo Research was used. Gene expression analysis for human samples was performed at the Institute for Research in Immunology and Cancer (IRIC) Genomics Core Facility, Université de Montréal. qRT-PCR analysis in APP/PS1 and WT mice was performed independently at Universidade Federal do Rio Grande do Sul and at Universidade Federal do Rio de Janeiro. Primers used for qRT-PCR

and result tables are listed in **Supplemental Table 6 and 7**. Standard scores (z-score) of APP/PS1, EOAD and LOAD were compared for their difference from control using Wilcoxon test in R statistical environment.

Acknowledgments

The results published here are partially based on data obtained from the AD Knowledge Portal (https://adknowledgeportal.synapse.org/). The IU/JAX and UCI MODEL-AD Center was established with funding from The National Institute on Aging (U54 AG054345-01 and AG054349). ERZ receives financial support from CNPq [435642/2018-9] and [312410/2018- 2], Instituto Serrapilheira [Serra-1912-31365], Brazilian National Institute of Science and Technology in Excitotoxicity and Neuroprotection [465671/2014-4], FAPERGS/MS/CNPq/SESRS–PPSUS [30786.434.24734.23112017] and ARD/FAPERGS [54392.632.30451.05032021]. MAB receives financial support from CNPq PDJ [150293/2019-4]. BB receives financial support from CAPES [88887.336490/2019-00]. Fundação Carlos Chagas Filho de Amparo à Pesquisa do Estado do Rio de Janeiro (FAPERJ) (202.744/2019 and 010.002421/2019 to MVL), Alzheimer's Association (AARG-D-615741 to MVL), and Serrapilheira Institute (R-2012-37967) funded experiments at the Lourenco lab. RASL-F is supported by a FAPERJ Nota Dez predoctoral scholarship.

Author Contributions

MAB selected the databases and performed transcriptomics analysis. MAB, BB and GC-C analyzed and interpreted the data and conceived figures and tables. BB, GC-C, RASL-F, MVL, MZ and PK collected experimental data. MAB and BB wrote the manuscript. ERZ conceived and supervised the project. GC-C, TAP, SF, ACM, RASL-F, MVL, PR-N and ERZ, edited and revised the manuscript for intellectual content.

Conflict of interest

Authors declare that they have no competing interests.

References

1. Reitz, C., Rogaeva, E. & Beecham, G. W. Late-onset vs nonmendelian early-onset Alzheimer disease: A distinction without a difference? *Neurol. Genet.* **6**, e512 (2020).
2. Cho, H. *et al.* Excessive tau accumulation in the parieto-occipital cortex characterizes early-onset Alzheimer's disease. *Neurobiol. Aging* **53**, 103–111 (2017).
3. McDade, E. *et al.* Longitudinal cognitive and biomarker changes in dominantly inherited Alzheimer disease. *Neurology* **91**, e1295–e1306 (2018).
4. Möller, C. *et al.* Different patterns of gray matter atrophy in early- and late-onset Alzheimer's disease. *Neurobiol. Aging* **34**, 2014–2022 (2013).
5. Rabinovici, G. D. *et al.* Increased metabolic vulnerability in early-onset Alzheimer's disease is not related to amyloid burden. *Brain* **133**, 512–528 (2010).
6. Schöll, M. *et al.* Distinct 18F-AV-1451 tau PET retention patterns in early- and late-onset Alzheimer's disease. *Brain* **140**, 2286–2294 (2017).
7. Morris, J. C. *et al.* Autosomal dominant and sporadic late onset Alzheimer disease share a common in vivo pathophysiology. *Brain* awac181 (2022) doi:10.1093/brain/awac181.
8. Saito, T., Matsuba, Y., Yamazaki, N., Hashimoto, S. & Saido, T. C. Calpain Activation in Alzheimer's Model Mice Is an Artifact of APP and Presenilin Overexpression. *J. Neurosci. Off. J. Soc. Neurosci.* **36**, 9933–9936 (2016).
9. Götz, J., Bodea, L.-G. & Goedert, M. Rodent models for Alzheimer disease. *Nat. Rev. Neurosci.* **19**, 583–598 (2018).
10. Saito, T. *et al.* Single App knock-in mouse models of Alzheimer's disease. *Nat. Neurosci.* **17**, 661–663 (2014).
11. Baglietto-Vargas, D. *et al.* Generation of a humanized Aβ expressing mouse demonstrating aspects of Alzheimer's disease-like pathology. *Nat. Commun.* **12**, 2421 (2021).
12. Serneels, L. *et al.* Modeling the β-secretase cleavage site and humanizing amyloid-beta precursor protein in rat and mouse to study Alzheimer's disease. *Mol. Neurodegener.* **15**, 60 (2020).
13. Ding, Q., Markesbery, W. R., Chen, Q., Li, F. & Keller, J. N. Ribosome dysfunction is an early event in Alzheimer's disease. *J. Neurosci. Off. J. Soc. Neurosci.* **25**, 9171–9175 (2005).
14. Gjoneska, E. *et al.* Conserved epigenomic signals in mice and humans reveal immune basis of Alzheimer's disease. *Nature* **518**, 365–369 (2015).
15. Hegde, A. N., Smith, S. G., Duke, L. M., Pourquoi, A. & Vaz, S. Perturbations of Ubiquitin-Proteasome-Mediated Proteolysis in Aging and Alzheimer's Disease. *Front. Aging Neurosci.* **11**, 324 (2019).
16. Thathiah, A. & De Strooper, B. The role of G protein-coupled receptors in the pathology of Alzheimer's disease. *Nat. Rev. Neurosci.* **12**, 73–87 (2011).
17. Lauretti, E., Dincer, O. & Praticò, D. Glycogen synthase kinase-3 signaling in Alzheimer's disease. *Biochim. Biophys. Acta - Mol. Cell Res.* **1867**, 118664 (2020).
18. Ledonne, A. *et al.* Neuregulin 1 signalling modulates mGluR1 function in mesencephalic dopaminergic neurons. *Mol. Psychiatry* **20**, 959–973 (2015).
19. Basu, A., Ash, P. E., Wolozin, B. & Emili, A. Protein Interaction Network Biology in Neuroscience. *Proteomics* **21**, e1900311 (2021).
20. Santiago, J. A., Bottero, V. & Potashkin, J. A. Dissecting the Molecular Mechanisms of Neurodegenerative Diseases through Network Biology. *Front. Aging Neurosci.* **9**, 166 (2017).
21. Gahete, M. D. *et al.* Expression of Somatostatin, cortistatin, and their receptors, as well as dopamine receptors, but not of neprilysin, are reduced in the temporal lobe of Alzheimer's disease patients. *J. Alzheimers. Dis.* **20**, 465–475 (2010).
22. Wang, H. *et al.* Somatostatin binds to the human amyloid β peptide and favors the formation of distinct oligomers. *Elife* **6**, (2017).
23. Nilsson, P. *et al.* Somatostatin receptor subtypes 1 and 4 redundantly regulate neprilysin, the major amyloid-beta degrading enzyme in brain. *bioRxiv* 2020.05.09.085795 (2020) doi:10.1101/2020.05.09.085795.

24. Burns, T. C., Li, M. D., Mehta, S., Awad, A. J. & Morgan, A. A. Mouse models rarely mimic the transcriptome of human neurodegenerative diseases: A systematic bioinformatics-based critique of preclinical models. *Eur. J. Pharmacol.* **759**, 101–117 (2015).
25. Tong, B. C.-K., Wu, A. J., Li, M. & Cheung, K.-H. Calcium signaling in Alzheimer's disease & therapies. *Biochim. Biophys. acta. Mol. cell Res.* **1865**, 1745–1760 (2018).
26. Tong, B. C.-K. *et al.* Familial Alzheimer's disease-associated presenilin 1 mutants promote γ-secretase cleavage of STIM1 to impair store-operated Ca2+ entry. *Sci. Signal.* **9**, ra89 (2016).
27. Frere, S. & Slutsky, I. Alzheimer's Disease: From Firing Instability to Homeostasis Network Collapse. *Neuron* **97**, 32–58 (2018).
28. Palop, J. J. & Mucke, L. Network abnormalities and interneuron dysfunction in Alzheimer disease. *Nat. Rev. Neurosci.* **17**, 777–792 (2016).
29. Horváth, A., Szűcs, A., Barcs, G., Noebels, J. L. & Kamondi, A. Epileptic Seizures in Alzheimer Disease: A Review. *Alzheimer Dis. Assoc. Disord.* **30**, 186–192 (2016).
30. Imfeld, P., Bodmer, M., Schuerch, M., Jick, S. S. & Meier, C. R. Seizures in patients with Alzheimer's disease or vascular dementia: a population-based nested case-control analysis. *Epilepsia* **54**, 700–707 (2013).
31. Verret, L. *et al.* Inhibitory interneuron deficit links altered network activity and cognitive dysfunction in Alzheimer model. *Cell* **149**, 708–721 (2012).
32. Martinez-Losa, M. *et al.* Nav1.1-Overexpressing Interneuron Transplants Restore Brain Rhythms and Cognition in a Mouse Model of Alzheimer's Disease. *Neuron* **98**, 75-89.e5 (2018).
33. Tong, L. M. *et al.* Inhibitory interneuron progenitor transplantation restores normal learning and memory in ApoE4 knock-in mice without or with Aβ accumulation. *J. Neurosci. Off. J. Soc. Neurosci.* **34**, 9506–9515 (2014).
34. Carro, M. S. *et al.* The transcriptional network for mesenchymal transformation of brain tumours. *Nature* **463**, 318–325 (2010).
35. Vargas, D. M., De Bastiani, M. A., Zimmer, E. R. & Klamt, F. Alzheimer's disease master regulators analysis: search for potential molecular targets and drug repositioning candidates. *Alzheimers. Res. Ther.* **10**, 59 (2018).
36. Lee, A., Shen, M. & Qiu, A. Psychiatric polygenic risk associates with cortical morphology and functional organization in aging. *Transl. Psychiatry* **7**, 1276 (2017).
37. Li, W. *et al.* FOXC2 often overexpressed in glioblastoma enhances proliferation and invasion in glioblastoma cells. *Oncol. Res.* **21**, 111–120 (2013).
38. Siegenthaler, J. A. *et al.* Foxc1 is required by pericytes during fetal brain angiogenesis. *Biol. Open* **2**, 647–659 (2013).
39. Liebl, J. *et al.* Cdk5 controls lymphatic vessel development and function by phosphorylation of Foxc2. *Nat. Commun.* **6**, 7274 (2015).
40. Kurbatskaya, K. *et al.* Upregulation of calpain activity precedes tau phosphorylation and loss of synaptic proteins in Alzheimer's disease brain. *Acta Neuropathol. Commun.* **4**, 34 (2016).
41. Ma, Y. *et al.* Activated cyclin-dependent kinase 5 promotes microglial phagocytosis of fibrillar β-amyloid by up-regulating lipoprotein lipase expression. *Mol. Cell. Proteomics* **12**, 2833–2844 (2013).
42. Seo, J. *et al.* Activity-dependent p25 generation regulates synaptic plasticity and Aβ-induced cognitive impairment. *Cell* **157**, 486–498 (2014).
43. Zheng, Y.-L. *et al.* A Cdk5 inhibitory peptide reduces tau hyperphosphorylation and apoptosis in neurons. *EMBO J.* **24**, 209–220 (2005).
44. Molofsky, A. V *et al.* Expression profiling of Aldh1l1-precursors in the developing spinal cord reveals glial lineage-specific genes and direct Sox9-Nfe2l1 interactions. *Glia* **61**, 1518–1532 (2013).
45. Nagao, M., Ogata, T., Sawada, Y. & Gotoh, Y. Zbtb20 promotes astrocytogenesis during neocortical development. *Nat. Commun.* **7**, 11102 (2016).
46. Stolt, C. C. *et al.* The Sox9 transcription factor determines glial fate choice in the

developing spinal cord. *Genes Dev.* **17**, 1677–1689 (2003).
47. Sun, W. *et al.* SOX9 Is an Astrocyte-Specific Nuclear Marker in the Adult Brain Outside the Neurogenic Regions. *J. Neurosci. Off. J. Soc. Neurosci.* **37**, 4493–4507 (2017).
48. Kumar, D. & Kumar, P. Aβ, Tau, and α-Synuclein aggregation and integrated role of PARK2 in the regulation and clearance of toxic peptides. *Neuropeptides* **78**, 101971 (2019).
49. Goiran, T. *et al.* β-Amyloid Precursor Protein Intracellular Domain Controls Mitochondrial Function by Modulating Phosphatase and Tensin Homolog-Induced Kinase 1 Transcription in Cells and in Alzheimer Mice Models. *Biol. Psychiatry* **83**, 416–427 (2018).
50. Martín-Maestro, P., Gargini, R., Perry, G., Avila, J. & García-Escudero, V. PARK2 enhancement is able to compensate mitophagy alterations found in sporadic Alzheimer's disease. *Hum. Mol. Genet.* **25**, 792–806 (2016).
51. Martín-Maestro, P. *et al.* Mitophagy Failure in APP and Tau Overexpression Model of Alzheimer's Disease. *J. Alzheimers. Dis.* **70**, 525–540 (2019).
52. Unger, M. S. *et al.* CD8(+) T-cells infiltrate Alzheimer's disease brains and regulate neuronal- and synapse-related gene expression in APP-PS1 transgenic mice. *Brain. Behav. Immun.* **89**, 67–86 (2020).
53. Blalock, E. M., Buechel, H. M., Popovic, J., Geddes, J. W. & Landfield, P. W. Microarray analyses of laser-captured hippocampus reveal distinct gray and white matter signatures associated with incipient Alzheimer's disease. *J. Chem. Neuroanat.* **42**, 118–126 (2011).
54. Miller, J. A., Woltjer, R. L., Goodenbour, J. M., Horvath, S. & Geschwind, D. H. Genes and pathways underlying regional and cell type changes in Alzheimer's disease. *Genome Med.* **5**, 48 (2013).
55. Hokama, M. *et al.* Altered expression of diabetes-related genes in Alzheimer's disease brains: the Hisayama study. *Cereb. Cortex* **24**, 2476–2488 (2014).
56. Berchtold, N. C. *et al.* Gene expression changes in the course of normal brain aging are sexually dimorphic. *Proc. Natl. Acad. Sci. U. S. A.* **105**, 15605–15610 (2008).
57. Wang, M. *et al.* Integrative network analysis of nineteen brain regions identifies molecular signatures and networks underlying selective regional vulnerability to Alzheimer's disease. *Genome Med.* **8**, 104 (2016).
58. Davis, S. & Meltzer, P. S. GEOquery: a bridge between the Gene Expression Omnibus (GEO) and BioConductor. *Bioinformatics* **23**, 1846–1847 (2007).
59. Leek, J. T., Johnson, W. E., Parker, H. S., Jaffe, A. E. & Storey, J. D. The sva package for removing batch effects and other unwanted variation in high-throughput experiments. *Bioinformatics* **28**, 882–883 (2012).
60. Voskuhl, R. R. *et al.* Gene expression in oligodendrocytes during remyelination reveals cholesterol homeostasis as a therapeutic target in multiple sclerosis. *Proc. Natl. Acad. Sci. U. S. A.* **116**, 10130–10139 (2019).
61. Soneson, C., Love, M. I. & Robinson, M. D. Differential analyses for RNA-seq: transcript-level estimates improve gene-level inferences. *F1000Research* **4**, 1521 (2015).
62. Ritchie, M. E. *et al.* limma powers differential expression analyses for RNA-sequencing and microarray studies. *Nucleic Acids Res.* **43**, e47 (2015).
63. Love, M. I., Huber, W. & Anders, S. Moderated estimation of fold change and dispersion for RNA-seq data with DESeq2. *Genome Biol.* **15**, 550 (2014).
64. Chen, H. & Boutros, P. C. VennDiagram: a package for the generation of highly-customizable Venn and Euler diagrams in R. *BMC Bioinformatics* **12**, 35 (2011).
65. Castro, M. A. A., Wang, X., Fletcher, M. N. C., Meyer, K. B. & Markowetz, F. RedeR: R/Bioconductor package for representing modular structures, nested networks and multiple levels of hierarchical associations. *Genome Biol.* **13**, R29 (2012).
66. Mora, A. & Donaldson, I. M. iRefR: an R package to manipulate the iRefIndex consolidated protein interaction database. *BMC Bioinformatics* **12**, 455 (2011).
67. Szklarczyk, D. *et al.* STRING v11: protein-protein association networks with increased

coverage, supporting functional discovery in genome-wide experimental datasets. *Nucleic Acids Res.* **47**, D607–D613 (2019).
68. Yu, G. *et al.* GOSemSim: an R package for measuring semantic similarity among GO terms and gene products. *Bioinformatics* **26**, 976–978 (2010).
69. Trabzuni, D. *et al.* Widespread sex differences in gene expression and splicing in the adult human brain. *Nat. Commun.* **4**, 2771 (2013).
70. Fletcher, M. N. C. *et al.* Master regulators of FGFR2 signalling and breast cancer risk. *Nat. Commun.* **4**, 2464 (2013).
71. Margolin, A. A. *et al.* Reverse engineering cellular networks. *Nat. Protoc.* **1**, 662–671 (2006).
72. Margolin, A. A. *et al.* ARACNE: an algorithm for the reconstruction of gene regulatory networks in a mammalian cellular context. *BMC Bioinformatics* **7 Suppl 1**, S7 (2006).
73. Subramanian, A. *et al.* Gene set enrichment analysis: a knowledge-based approach for interpreting genome-wide expression profiles. *Proc. Natl. Acad. Sci. U. S. A.* **102**, 15545–15550 (2005).
74. Alvarez, M. J. *et al.* Functional characterization of somatic mutations in cancer using network-based inference of protein activity. *Nat. Genet.* **48**, 838–847 (2016).

Figure legends

Figure 1 | Shared DEGs among EOAD, LOAD and mouse models of AD. Venn diagram showing DEGs overlap between EOAD **(A)** and LOAD **(B)** with 5xFAD, APP/PS1 and hAβ-KI mice. Mosaic plot of hAβ-KI, 5xFAD, and APP/PS1 overlap **(C)**. Mosaic plot of EOAD-model (left) and model-EOAD (right) DEGs overlap with 5xFAD, APP/PS1, and hAβ-KI mice **(D)**. Mosaic plot of LOAD-model (left) and model-LOAD (right) DEGs overlap with 5xFAD, APP/PS1 and hAβ-KI mice **(E)**. PPI network of DEGs exclusively shared between hAβ-KI mice and LOAD **(F)** or EOAD **(G)** patients. Mosaic plot of EOAD, LOAD or MS DEGs overlap with 5xFAD mice **(H)**. Mosaic plot of EOAD, LOAD or MS DEGs overlap with APP/PS1 mice **(I)**. Mosaic plot of EOAD, LOAD or MS DEGs overlap with hAβ-KI mice **(J)**. The size of red and yellow boxes reflects the proportion of overlapping and non-overlapping DEGs, respectively. Pearson's Chi−squared test with Yates' continuity correction was applied for the mosaic plot analysis. EOAD = early-onset Alzheimer's disease; LOAD = late-onset Alzheimer's disease; MS = multiple sclerosis; hAβ-KI = humanized amyloid-β knock-in. Genes with unadjusted p-value < 0.05 were considered as DEGs.

Figure 2 | Experimental validation of exploratory transcriptomics findings. The seven genes overlapping between AD and animal models were evaluated in hippocampus from APP/PS1 (n = 14) and WT (n= 14) mice from two independent laboratories **(A)** and in cognitively unimpaired (CU, n = 9), early- (EOAD, n = 7) and late-onset Alzheimer's disease (LOAD, n = 8) patients from the Douglas-Bell Canada Brain Bank **(B)**. Standard scores (z-score) of APP/PS1, EOAD and LOAD were compared for their difference from control using Wilcoxon.

Figure 3 | GOBP overlap among EOAD, LOAD, and mouse models of AD. Venn diagram of GOBPs intersections in EOAD **(A)** and LOAD **(B)** with 5xFAD, APP/PS1 and hAβ-KI mice. Mosaic plot of hAβ-KI-5xFAD and -APP/PS1 GOBP overlap **(C)**. Mosaic plot of EOAD-model (left) and model-EOAD (right) GOBP overlap with 5xFAD, APP/PS1, and hAβ-KI mice **(D)**.

Mosaic plot of LOAD-model (left) and model-LOAD (right) GOBP overlap with 5xFAD, APP/PS1 and hAβ-KI mice **(E)**. Mosaic plot of EOAD, LOAD, or MS GOBP overlap with 5xFAD mice **(F)**. Mosaic plot of EOAD, LOAD, or MS GOBP overlap with APP/PS1 mice **(G)**. Mosaic plot of EOAD, LOAD, or MS GOBP overlap with hAβ-KI mice **(H)**. The size of the red and yellow boxes reflects the proportion of overlapping and non-overlapping GOBPs, respectively. Pearson's Chi−squared test with Yates' continuity correction was applied for the mosaic plot analysis. EOAD = early-onset Alzheimer's disease; LOAD = late-onset Alzheimer's disease; MS = multiple sclerosis; hAβ-KI = humanized amyloid-β knock-in.

Figure 4 | Nested networks of enriched GOBP intersections between EOAD and AD mouse models. Blue, purple and orange circles represent the overlap between EOAD and protein overexpression mouse models. Intersection among EOAD and hAβ-KI is represented by circles in shades of gray. Each box represents a cluster of GOBP terms grouped by semantic similarity and named manually according to its main biological role. Circle sizes represent the number of genes enriched in the GO term. EOAD = early-onset Alzheimer's disease; MS = multiple sclerosis; hAβ-KI = humanized amyloid-β knock-in.

Figure 5 | Nested networks of enriched GOBP intersections between LOAD and AD mouse models. Light purple, dark purple, and green circles represent all the GOBP terms overlap between LOAD and hAβ-KI. Intersection among LOAD and overexpression protein mouse models is represented by circles in shades of gray. Each box represents a cluster of GOBP terms grouped by semantic similarity and named manually according to its main biological role. Circle sizes represent the number of genes enriched in the GO term. LOAD = late-onset Alzheimer's disease; MS = multiple sclerosis; hAβ-KI = humanized amyloid-β knock-in.

Figure 6 | Functional enrichment analysis of KEGG terms in mouse models of AD and human disease. Venn diagrams showing the KEGGs overlap among EOAD **(A)** and LOAD **(B)** patients with 5xFAD, APP/PS1 and hAβ-KI mice. Mosaic plot of 5xFAD, APP/PS1 and hAβ-KI KEGGs overlap with EOAD **(C)** or LOAD **(D)**. Dual-plots showing the up- (red) and down- (blue) regulated KEGGs for EOAD **(E)**, LOAD **(F)**, 5xFAD **(G)**, APP/PS1 **(H)** and hAβ-KI **(I)**.

The size of the red and yellow boxes reflects the proportion of overlapping and non-overlapping KEGGs, respectively. Pearson's Chi−squared test with Yates' continuity correction was applied for the mosaic plot analysis. The pathways in the dual-plots are represented in the Y axis; the left and the right part of the X axis corresponds to the number of genes enriched in the KEGG terms and their q-value (grey bars), respectively. EOAD = early-onset Alzheimer's disease; LOAD = late-onset Alzheimer's disease; MS = multiple sclerosis; hAβ-KI = humanized amyloid-β knock-in.

Figure 7 | Master regulator analysis of mouse models of AD and human disease. Venn diagrams of EOAD **(A)** or LOAD **(B)** with 5xFAD, APP/PS1, and hAβ-KI MRs overlap. Tile-plot of regulons significantly enriched with DEGs in EOAD, LOAD, 5xFAD, APP/PS1 and hAβ-KI (only regulatory units significant in ≥ 4 contexts are represented) **(C)**. Tile-plot showing the activation state of the transcription factors acting as MR in EOAD, LOAD, 5xFAD, APP/PS1, and hAβ-KI **(D)**. Venn diagram showing the overlap between previously MR candidates found by Vargas et al. and the current study **(E)**. EOAD = early-onset Alzheimer's disease; LOAD = late-onset Alzheimer's disease; hAβ-KI = humanized amyloid-β knock-in; ns = non-significant.

Figure 8 | Phenotypic features of AD mouse models, AD diagnosis, control group definition, and demographics of human samples. APP/PS1 (top), 5xFAD (middle) and hAβ-KI mice (bottom) timelines showing specific phenotypes of each mouse model across different ages (in months (**A**). Numbers in bold correspond to the time points evaluated in this study. Data for APP/PS1 and 5xFAD mice were obtained at AlzForum. hAβ-KI information was taken from Baglietto-Vargas et al (Baglietto-Vargas *et al.*, 2021). The individuals were diagnosed with AD according to established clinical criteria and/or neuropathological *post-mortem* evaluation in each selected GSE study **(B)**. Age, sample size and sex information are specified for EOAD, LOAD and MS patients and their age-matched controls **(C)**. NINCDS-ADRDA 1984 (McKhann *et al*, 1984); CERAD (Mirra *et al*, 1991); NIA-Reagan Institute criteria (Hyman, 1997); Braak staging (Braak & Braak, 1991); NFT = neurofibrillary tangles; MMSE =

Mini-Mental State Examination; DLB = Dementia with Lewy bodies; PD = Parkinson’s disease; MS = Multiple Sclerosis. EOAD = early-onset Alzheimer's disease; LOAD = late-onset Alzheimer's disease.

Supplemental Figure Legends

Figure S1 | DEGs in mouse models of AD and human disease. Volcano plots and pie charts showing the up- and down-regulated genes in 5xFAD **(A)**, APP/PS1 **(B)**, hAβ-KI **(C)**, EOAD **(D)**, LOAD **(E)** and MS individuals **(F)**. Red points in volcano plots correspond to a DEG when compared to control. In pie charts, pink and blue colors correspond respectively to the up- and down-regulated DEGs. EOAD = early-onset Alzheimer's disease; LOAD = late-onset Alzheimer's disease; MS = multiple sclerosis; hAβ-KI = human amyloid-β knock-in. Genes with unadjusted p-value < 0.05 were considered as DEGs.

Figure S2 | Intersection of DEGs between animal models and AD subtypes. Mosaic plot of EOAD-model **(A)** and model-EOAD **(B)** DEGs overlap with 5xFAD, APP/PS1 and hAβ-KI mice. Genes with *BH adjusted p-value < 0.1* were considered as DEGs in the mosaic plots.

Figure S3 | Shared DEGs and enriched GOBP among mouse models of AD and human disease. Venn diagrams showing the DEGs (left) and GOBP terms (right) overlap among 5xFAD **(A, D)**, APP/PS1 **(B, E)** and hAβ-KI **(C, F)** mice with EOAD, LOAD and MS individuals. EOAD = early-onset Alzheimer's disease; LOAD = late-onset Alzheimer's disease; MS = multiple sclerosis; hAβ-KI = human amyloid-β knock-in. Genes with unadjusted p-value < 0.05 were selected as DEGs.

Figure S4 | VIPER analysis of EOAD, LOAD and AD mouse models. Plot of inferred regulon activity showing the up- (reddish) and down- (bluish) regulated transcription factors in each group: EOAD **(A)**, LOAD **(B)**, 5xFAD **(C)**, APP/PS1 **(D)** and hAβ-KI **(E)**. EOAD = early-onset Alzheimer's disease; LOAD = late-onset Alzheimer's disease; hAβ-KI = human amyloid-β knock-in. *p-value < 0.05

DIFFERENTIALLY EXPRESSED GENES

A)

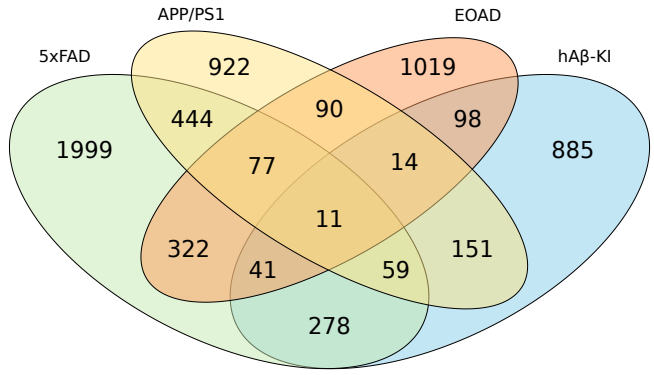

B)

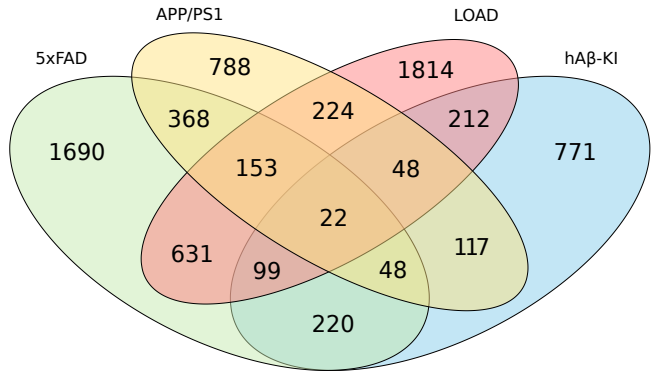

C)

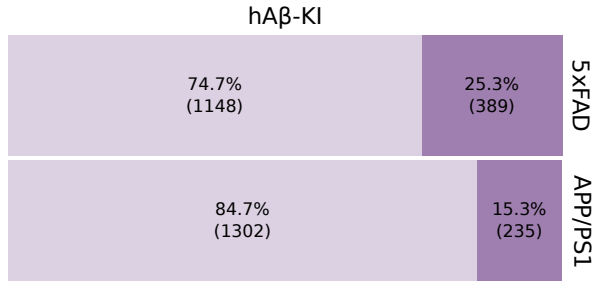

X^2 = 47.07; p−value <0.001

D)

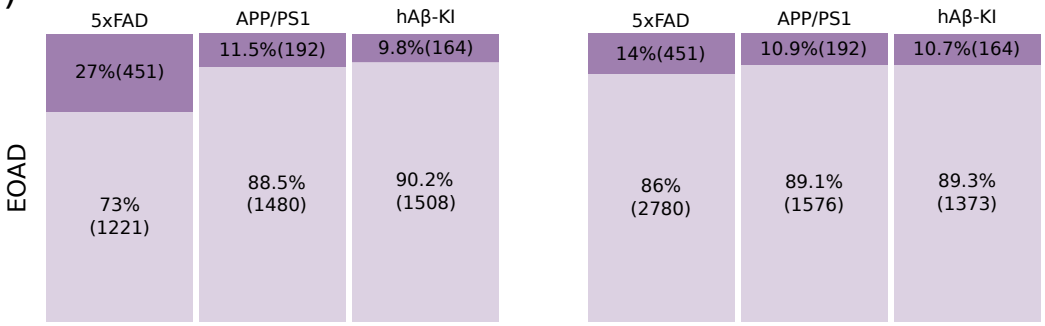

Disease−Model Overlap

X^2 = 221.86; p−value < 0.001

Pairwise Comparison	raw.p	adj.p
5xFAD vs APP/PS1	<0.001	<0.001
5xFAD vs hAβ-KI	<0.001	<0.001
APP/PS1 vs hAβ-KI	0.1301	0.3902

Model−Disease Overlap

X^2 = 15.36; p−value < 0.001

Pairwise Comparison	raw.p	adj.p
5xFAD vs APP/PS1	0.002	0.0061
5xFAD vs hAβ-KI	0.0018	0.0054
APP/PS1 vs hAβ-KI	0.9097	1

E)

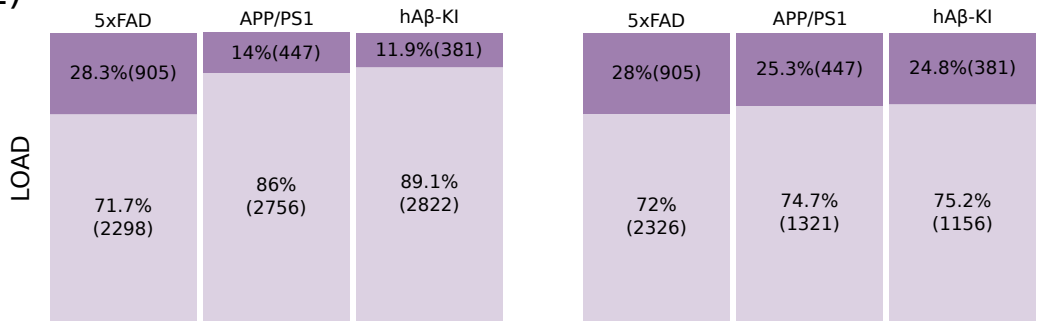

Disease−Model Overlap

X^2 = 344.04; p−value < 0.001

Pairwise Comparison	raw.p	adj.p
5xFAD vs APP/PS1	<0.001	<0.001
5xFAD vs hAβ-KI	<0.001	<0.001
APP/PS1 vs hAβ-KI	0.0155	0.0465

Model−Disease Overlap

X^2 = 7.43; p−value = 0.0243

Pairwise Comparison	raw.p	adj.p
5xFAD vs APP/PS1	0.0411	0.1234
5xFAD vs hAβ-KI	0.0210	0.0631
APP/PS1 vs hAβ-KI	0.7742	1

F)

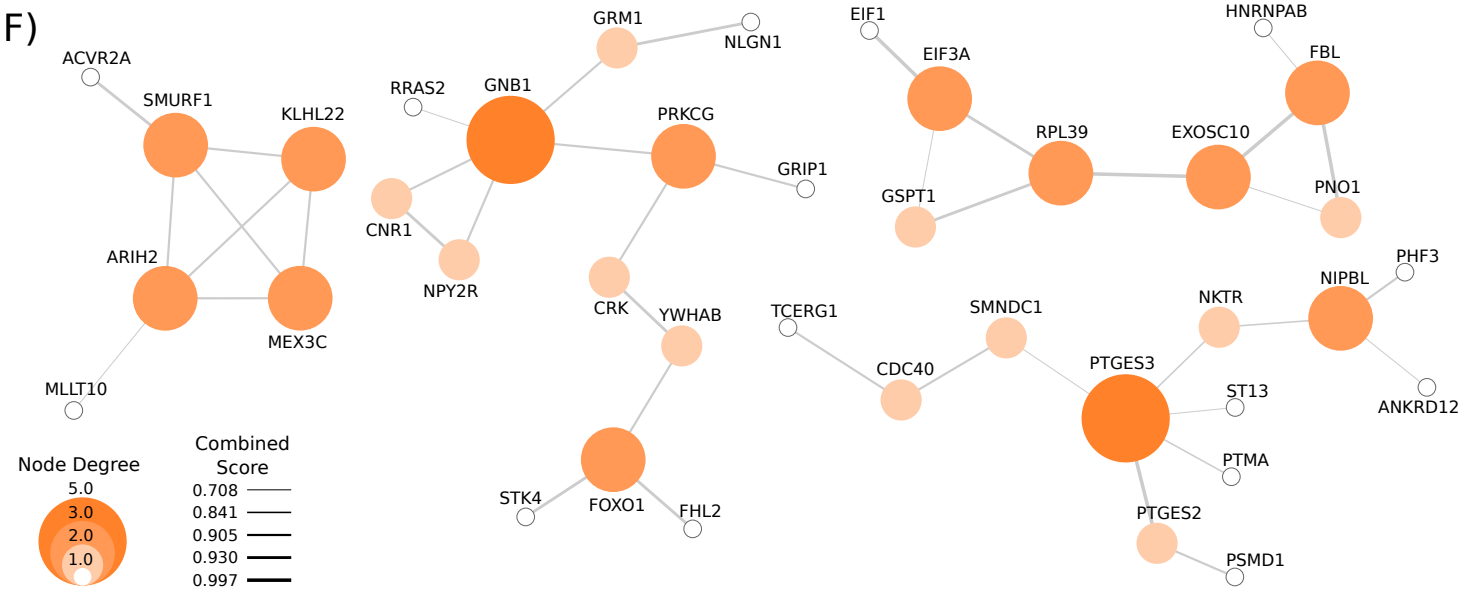

G)

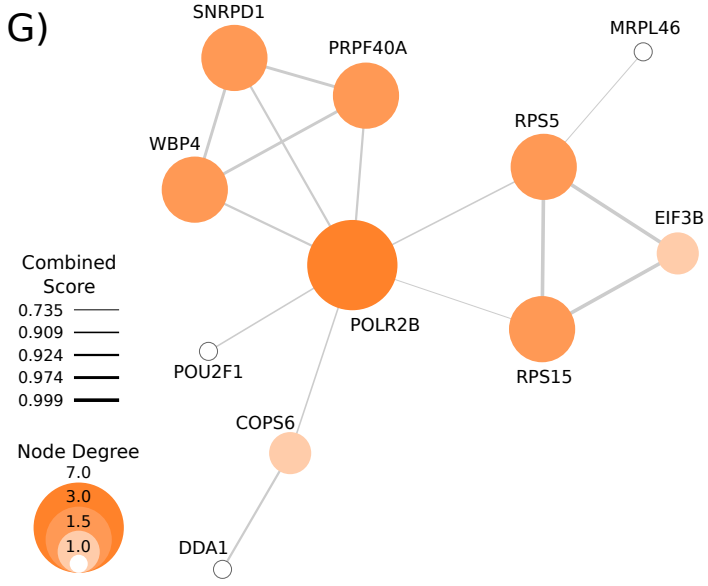

H)

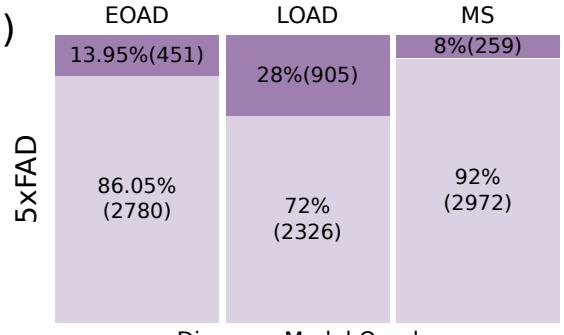

Disease−Model Overlap

X^2 = 490.56; p−value < 0.001

Pairwise Comparison	raw.p	adj.p
EOAD vs LOAD	<0.001	<0.001
EOAD vs MS	<0.001	<0.001
LOAD vs MS	<0.001	<0.001

I)

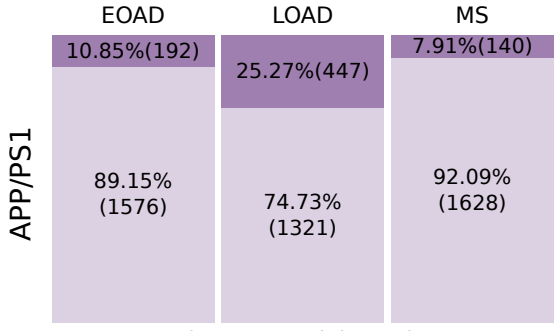

Disease−Model Overlap

X^2 = 243.7; p−value < 0.001

Pairwise Comparison	raw.p	adj.p
EOAD vs LOAD	<0.001	<0.001
EOAD vs MS	0.0033	0.0098
LOAD vs MS	<0.001	<0.001

J)

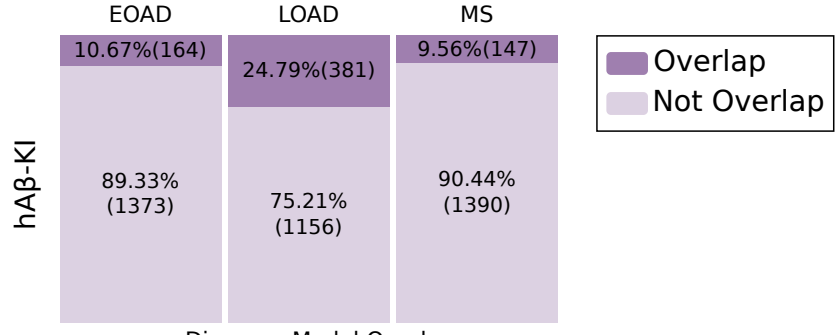

Disease−Model Overlap

X^2 = 173.65; p−value < 0.001

Pairwise Comparison	raw.p	adj.p
EOAD vs LOAD	<0.001	<0.001
EOAD vs MS	0.3386	1
LOAD vs MS	<0.001	<0.001

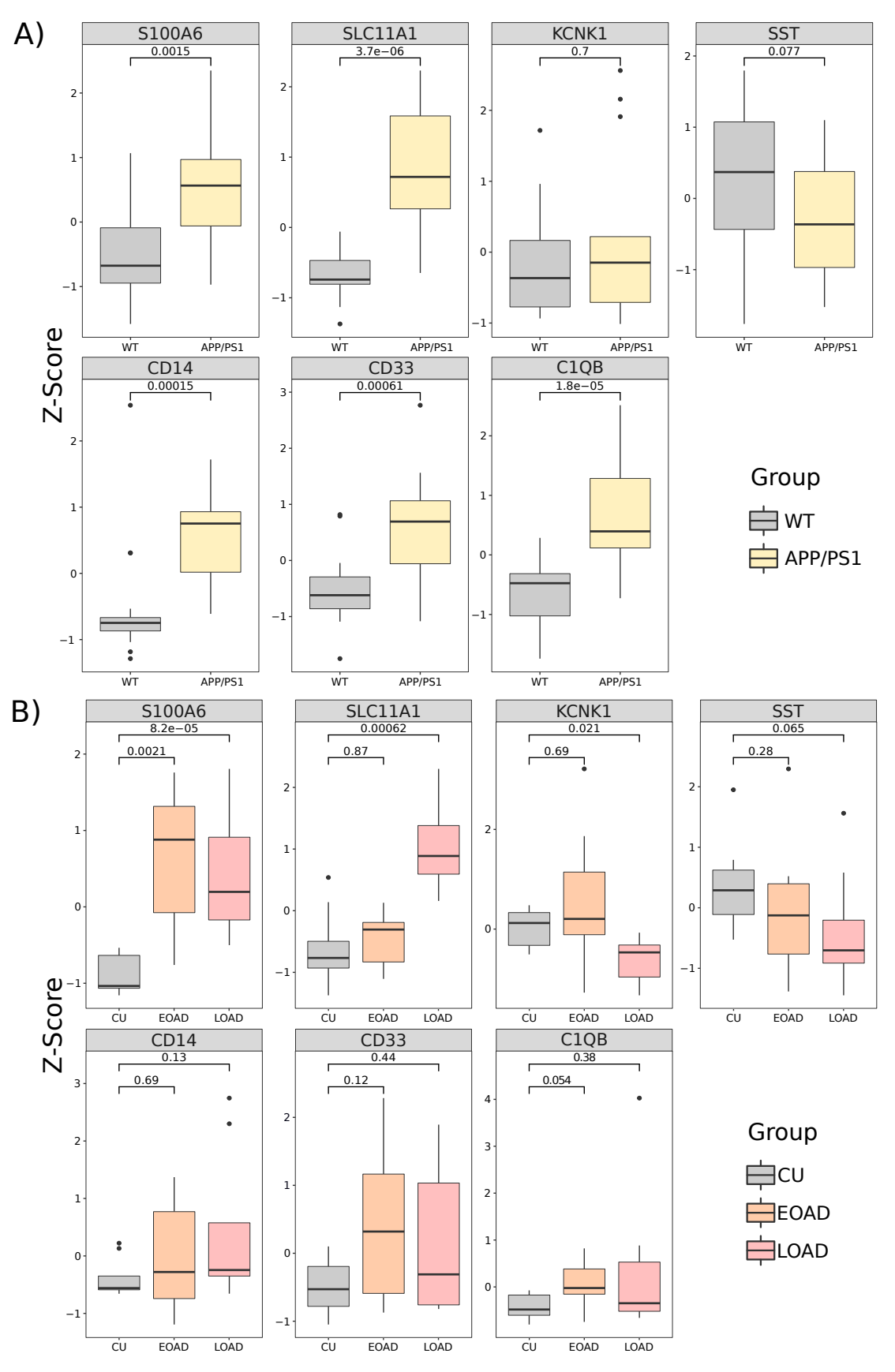
A)
S100A6
0.0015
SLC11A1
3.7e−06
KCNK1
0.7
SST
0.077
CD14
0.00015
CD33
0.00061
C1QB
1.8e−05
Z-Score
WT
APP/PS1
Group
WT
APP/PS1
B)
S100A6
8.2e−05
0.0021
SLC11A1
0.00062
0.87
KCNK1
0.021
0.69
SST
0.065
0.28
CD14
0.13
0.69
CD33
0.44
0.12
C1QB
0.38
0.054
Z-Score
CU
EOAD
LOAD
Group
CU
EOAD
LOAD

GENE ONTOLOGY BIOLOGICAL PROCESS

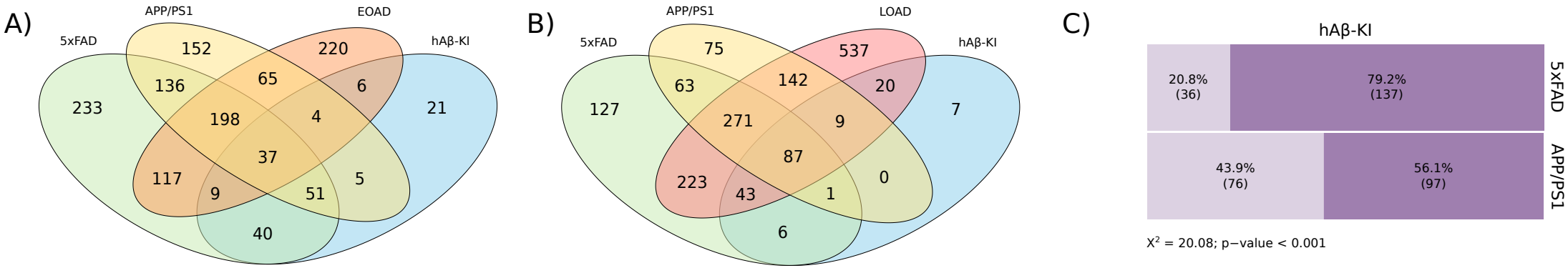

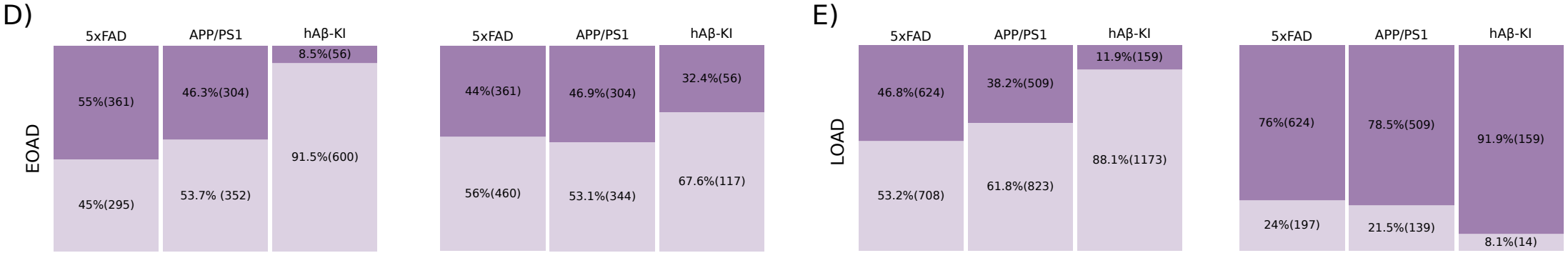

Pairwise Comparison	raw.p	adj.p
5xFAD vs APP/PS1	0.002	0.006
5xFAD vs hAβ-KI	<0.001	<0.001
APP/PS1 vs hAβ-KI	<0.001	<0.001

Pairwise Comparison	raw.p	adj.p
5xFAD vs APP/PS1	0.2836	0.8507
5xFAD vs hAβ-KI	0.0064	0.0193
APP/PS1 vs hAβ-KI	0.0008	0.0025

Pairwise Comparison	raw.p	adj.p
5xFAD vs APP/PS1	<0.001	<0.001
5xFAD vs hAβ-KI	<0.001	<0.001
APP/PS1 vs hAβ-KI	<0.001	<0.001

Pairwise Comparison	raw.p	adj.p
5xFAD vs APP/PS1	0.2756	0.8267
5xFAD vs hAβ-KI	<0.001	<0.001
APP/PS1 vs hAβ-KI	0.0001	0.0003

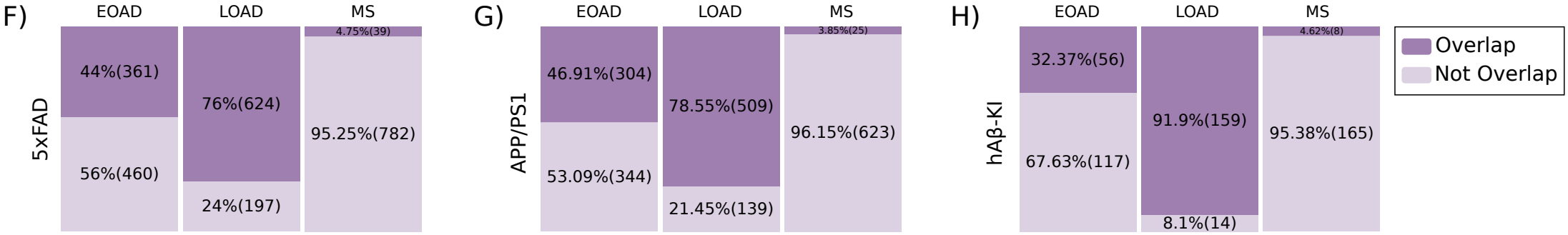

Pairwise Comparison	raw.p	adj.p
EOAD vs LOAD	<0.001	<0.001
EOAD vs MS	<0.001	<0.001
LOAD vs MS	<0.001	<0.001

Pairwise Comparison	raw.p	adj.p
EOAD vs LOAD	<0.001	<0.001
EOAD vs MS	<0.001	<0.001
LOAD vs MS	<0.001	<0.001

Pairwise Comparison	raw.p	adj.p
EOAD vs LOAD	<0.001	<0.001
EOAD vs MS	<0.001	<0.001
LOAD vs MS	<0.001	<0.001

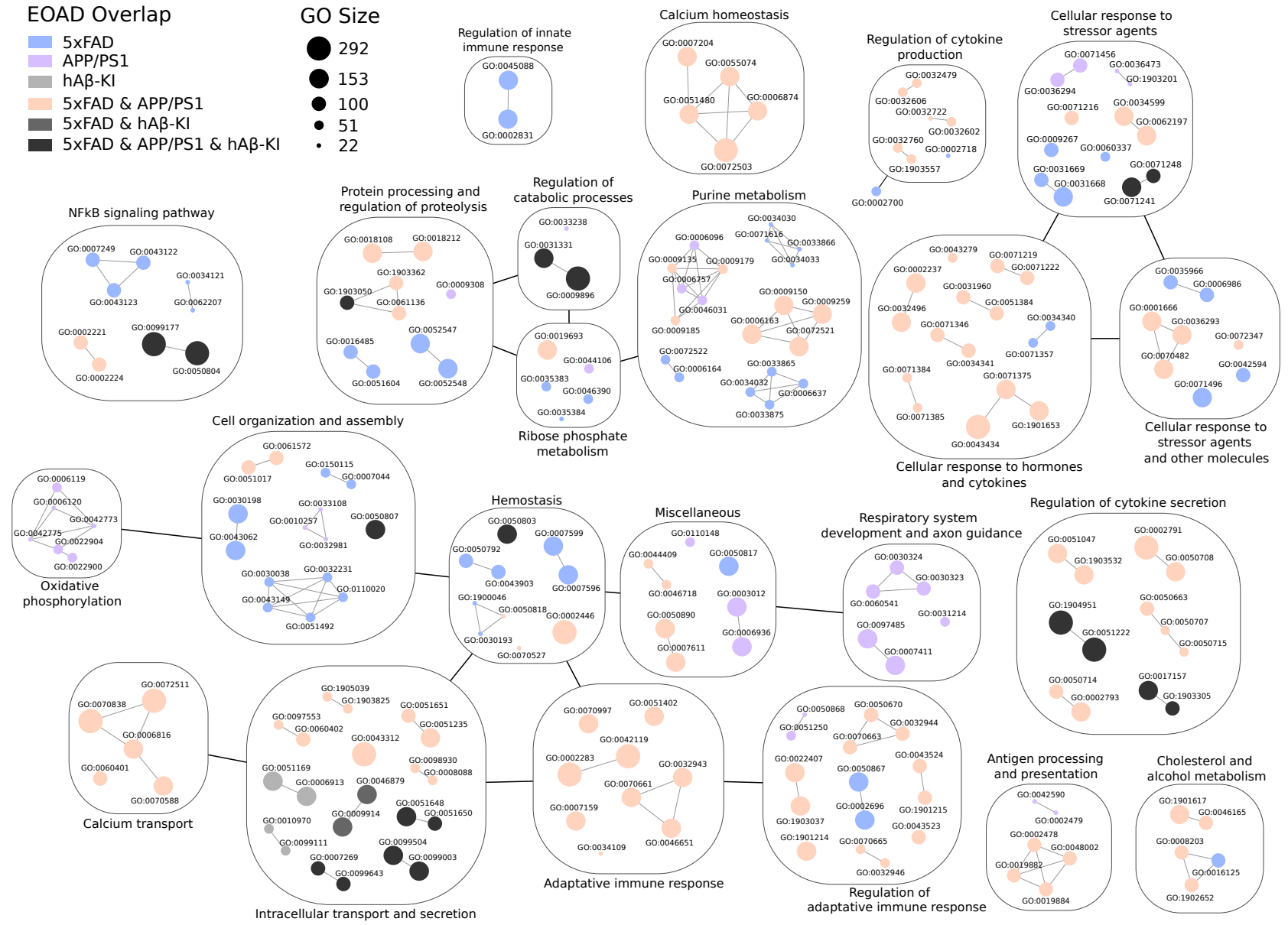
EOAD Overlap
5xFAD
APP/PS1
hAβ-KI
5xFAD & APP/PS1
5xFAD & hAβ-KI
5xFAD & APP/PS1 & hAβ-KI
GO Size
292
153
100
51
22
Regulation of innate immune response
GO:0045088
GO:0002831
Calcium homeostasis
GO:0007204
GO:0055074
GO:0051480
GO:0006874
GO:0072503
Regulation of cytokine production
GO:0032479
GO:0032606
GO:0032722
GO:0032602
GO:0032760
GO:0002718
GO:1903557
GO:0002700
Cellular response to stressor agents
GO:0071456
GO:0036473
GO:1903201
GO:0036294
GO:0071216
GO:0034599
GO:0062197
GO:0009267
GO:0060337
GO:0071248
GO:0031669
GO:0031668
GO:0071241
NFkB signaling pathway
GO:0007249
GO:0043122
GO:0034121
GO:0043123
GO:0062207
GO:0002221
GO:0099177
GO:0050804
GO:0002224
Protein processing and regulation of proteolysis
GO:0018108
GO:0018212
GO:1903362
GO:0009308
GO:1903050
GO:0061136
GO:0052547
GO:0016485
GO:0051604
GO:0052548
Regulation of catabolic processes
GO:0033238
GO:0031331
GO:0009896
GO:0019693
GO:0044106
GO:0035383
GO:0046390
GO:0035384
Ribose phosphate metabolism
Purine metabolism
GO:0034030
GO:0006096
GO:0071616
GO:0033866
GO:0009135
GO:0009179
GO:0034033
GO:0006257
GO:0009150
GO:0009259
GO:0046031
GO:0006163
GO:0009185
GO:0072521
GO:0072522
GO:0033865
GO:0006164
GO:0034032
GO:0006637
GO:0033875
GO:0043279
GO:0071219
GO:0002237
GO:0071222
GO:0031960
GO:0032496
GO:0051384
GO:0071346
GO:0034340
GO:0071357
GO:0034341
GO:0071384
GO:0071375
GO:0071385
GO:1901653
GO:0043434
Cellular response to hormones and cytokines
GO:0035966
GO:0006986
GO:0001666
GO:0036293
GO:0072347
GO:0070482
GO:0042594
GO:0071496
Cellular response to stressor agents and other molecules
Cell organization and assembly
GO:0061572
GO:0150115
GO:0051017
GO:0007044
GO:0030198
GO:0033108
GO:0010257
GO:0050807
GO:0043062
GO:0032981
GO:0030038
GO:0032231
GO:0110020
GO:0043149
GO:0051492
GO:0006119
GO:0006120
GO:0042773
GO:0042775
GO:0022904
GO:0022900
Oxidative phosphorylation
Hemostasis
GO:0050803
GO:0007599
GO:0050792
GO:0043903
GO:0007596
GO:1900046
GO:0050818
GO:0002446
GO:0030193
GO:0070527
Miscellaneous
GO:0110148
GO:0044409
GO:0050817
GO:0046718
GO:0003012
GO:0050890
GO:0006936
GO:0007611
Respiratory system development and axon guidance
GO:0030324
GO:0030323
GO:0060541
GO:0031214
GO:0097485
GO:0007411
Regulation of cytokine secretion
GO:0051047
GO:0002791
GO:1903532
GO:0050708
GO:1904951
GO:0050663
GO:0050707
GO:0051222
GO:0050715
GO:0050714
GO:0017157
GO:0002793
GO:1903305
GO:0072511
GO:0070838
GO:0006816
GO:0060401
GO:0070588
Calcium transport
GO:1905039
GO:1903825
GO:0051651
GO:0097553
GO:0060402
GO:0051235
GO:0043312
GO:0098930
GO:0008088
GO:0051169
GO:0006913
GO:0046879
GO:0051648
GO:0009914
GO:0051650
GO:0010970
GO:0099111
GO:0099504
GO:0007269
GO:0099003
GO:0099643
Intracellular transport and secretion
GO:0070997
GO:0051402
GO:0042119
GO:0002283
GO:0032943
GO:0070661
GO:0007159
GO:0034109
GO:0046651
Adaptative immune response
GO:0050868
GO:0050670
GO:0051250
GO:0032944
GO:0070663
GO:0022407
GO:0043524
GO:0050867
GO:0002696
GO:1901215
GO:1903037
GO:0043523
GO:1901214
GO:0070665
GO:0032946
Regulation of adaptative immune response
Antigen processing and presentation
GO:0042590
GO:0002479
GO:0002478
GO:0048002
GO:0019882
GO:0019884
Cholesterol and alcohol metabolism
GO:1901617
GO:0046165
GO:0008203
GO:0016125
GO:1902652

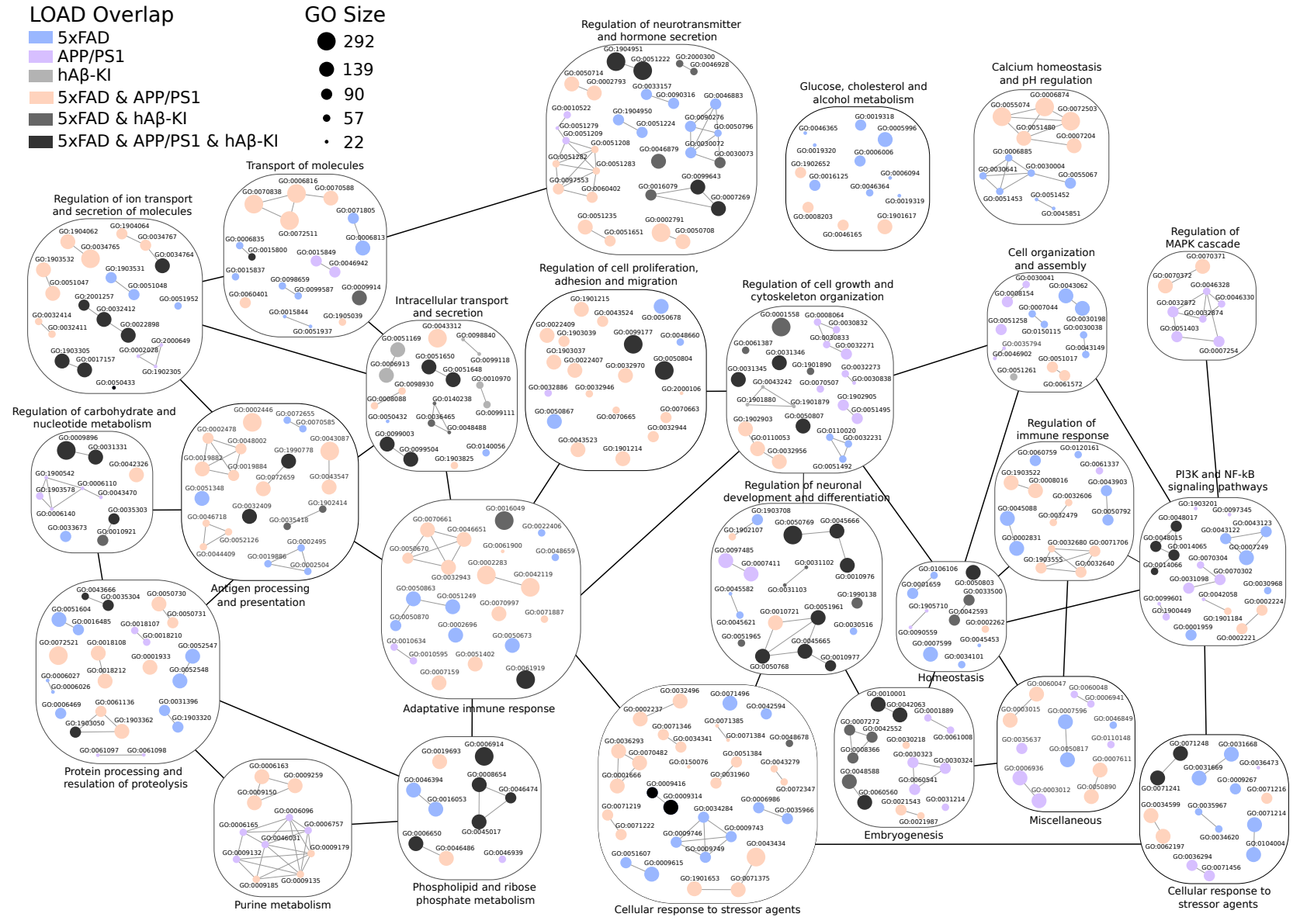
LOAD Overlap
5xFAD
APP/PS1
hAβ-KI
5xFAD & APP/PS1
5xFAD & hAβ-KI
5xFAD & APP/PS1 & hAβ-KI
GO Size
292
139
90
57
22
Regulation of neurotransmitter and hormone secretion
Glucose, cholesterol and alcohol metabolism
Calcium homeostasis and pH regulation
Transport of molecules
Regulation of ion transport and secretion of molecules
Regulation of MAPK cascade
Regulation of cell proliferation, adhesion and migration
Cell organization and assembly
Regulation of cell growth and cytoskeleton organization
Intracellular transport and secretion
Regulation of carbohydrate and nucleotide metabolism
Regulation of immune response
Regulation of neuronal development and differentiation
PI3K and NF-kB signaling pathways
Antigen processing and presentation
Homeostasis
Adaptative immune response
Protein processing and resulation of proteolysis
Embryogenesis
Miscellaneous
Purine metabolism
Phospholipid and ribose phosphate metabolism
Cellular response to stressor agents
Cellular response to stressor agents

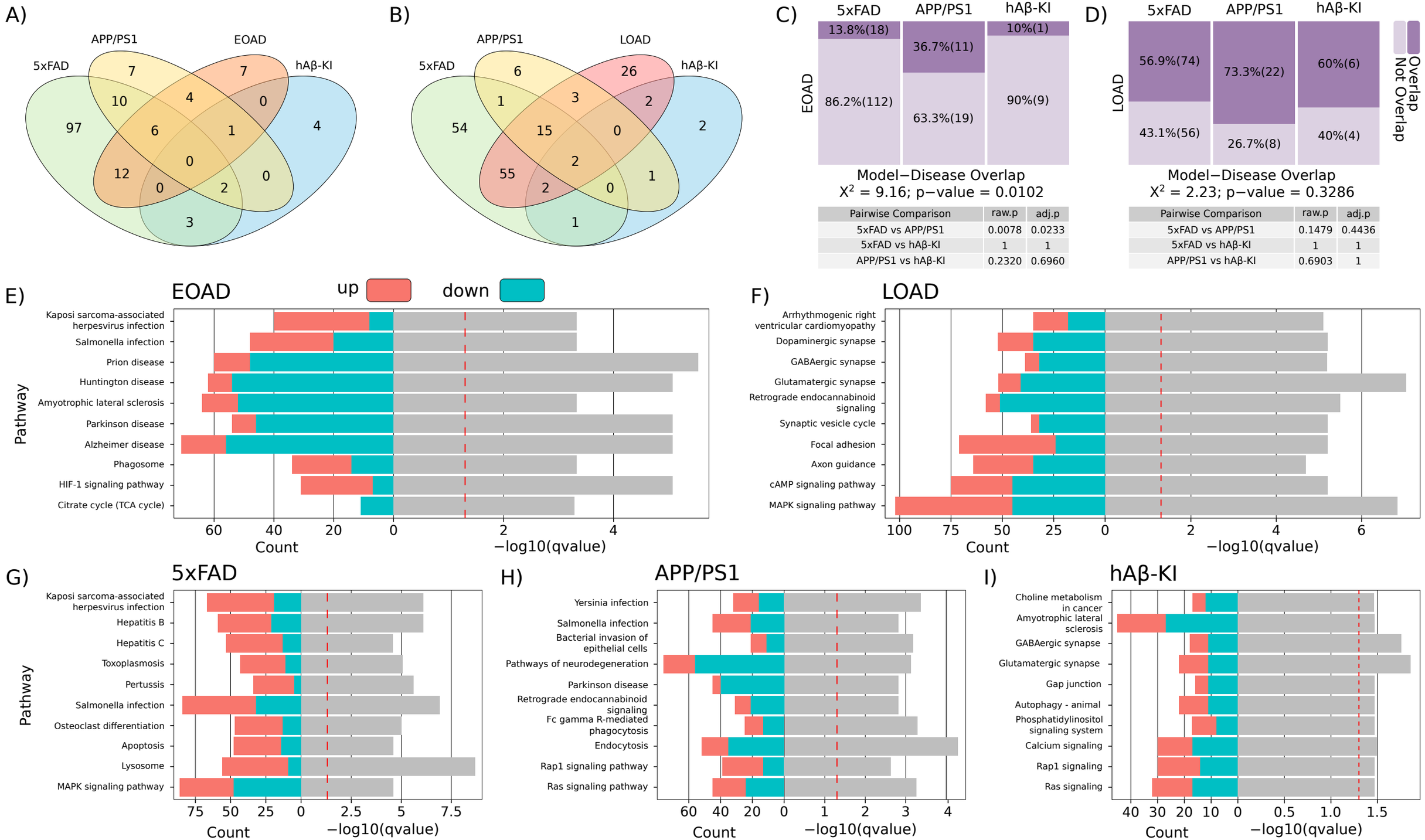

Pairwise Comparison	raw.p	adj.p
5xFAD vs APP/PS1	0.0078	0.0233
5xFAD vs hAβ-KI	1	1
APP/PS1 vs hAβ-KI	0.2320	0.6960

Pairwise Comparison	raw.p	adj.p
5xFAD vs APP/PS1	0.1479	0.4436
5xFAD vs hAβ-KI	1	1
APP/PS1 vs hAβ-KI	0.6903	1

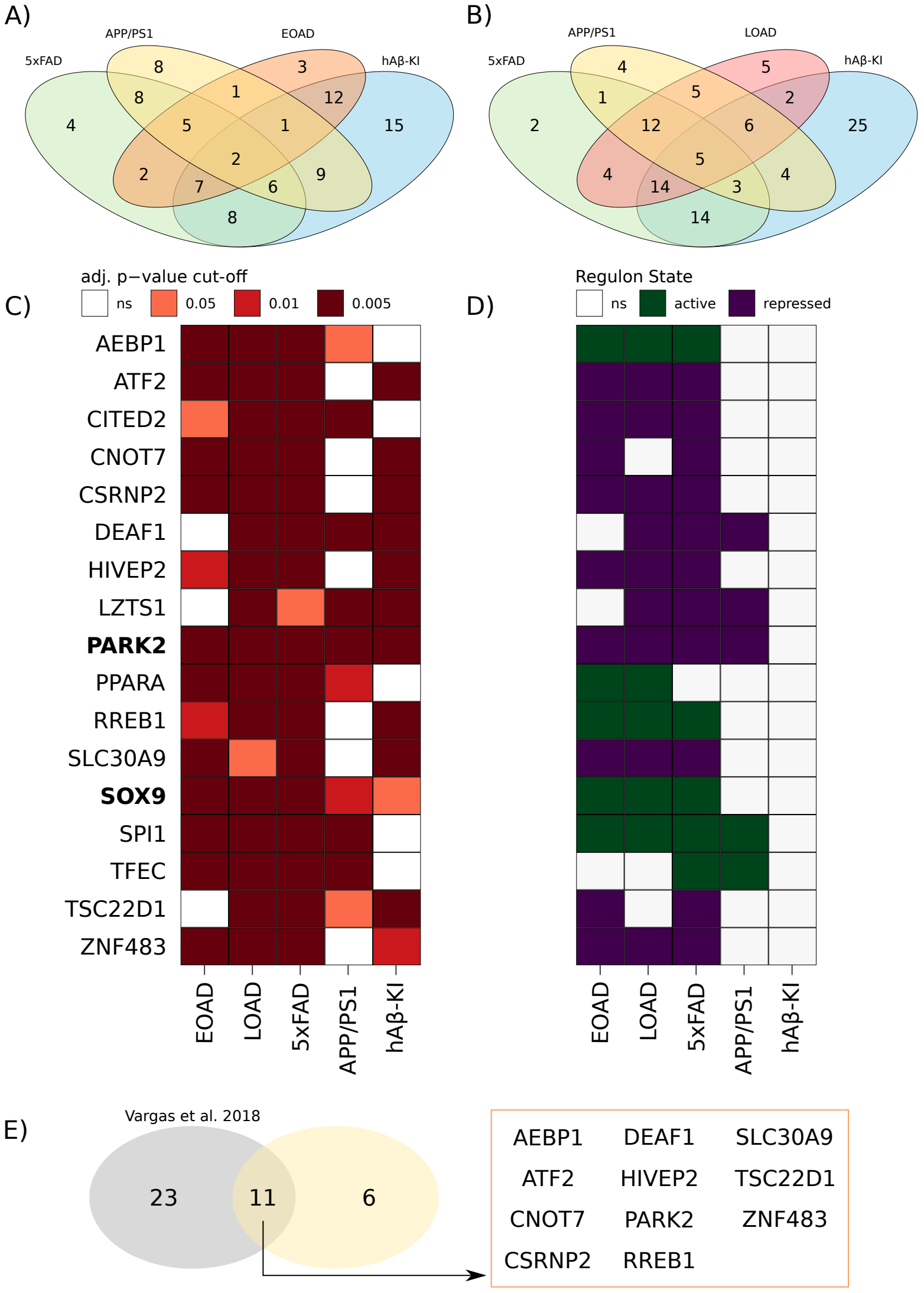
A)
APP/PS1
EOAD
5xFAD
hAβ-KI
8
3
8
1
12
4
5
1
15
2
2
7
6
9
8
B)
APP/PS1
LOAD
5xFAD
hAβ-KI
4
5
1
5
2
2
12
6
25
5
4
14
3
4
14
C)
adj. p−value cut-off
ns
0.05
0.01
0.005
AEBP1
ATF2
CITED2
CNOT7
CSRNP2
DEAF1
HIVEP2
LZTS1
PARK2
PPARA
RREB1
SLC30A9
SOX9
SPI1
TFEC
TSC22D1
ZNF483
EOAD
LOAD
5xFAD
APP/PS1
hAβ-KI
D)
Regulon State
ns
active
repressed
EOAD
LOAD
5xFAD
APP/PS1
hAβ-KI
E)
Vargas et al. 2018
23
11
6
AEBP1
ATF2
CNOT7
CSRNP2
DEAF1
HIVEP2
PARK2
RREB1
SLC30A9
TSC22D1
ZNF483

A)

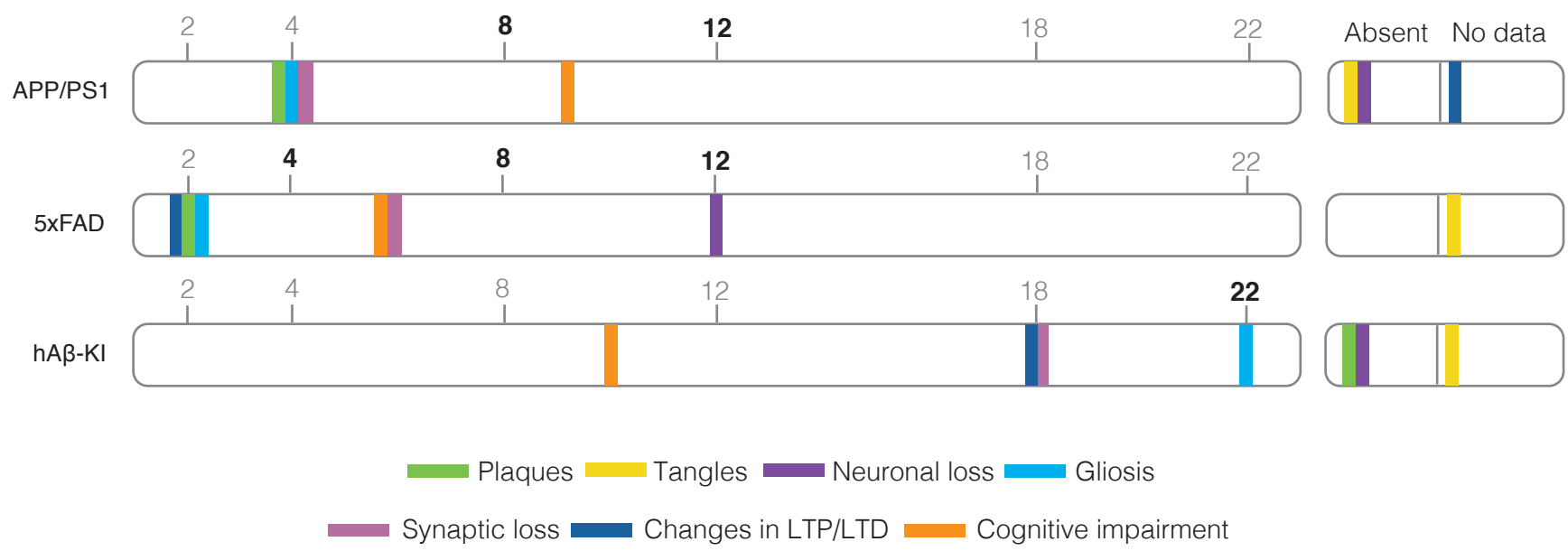

B)

AD diagnosis and control definition			
GSE	AD diagnosis	Control definition	Exclusion criteria
28146	NINCDS-ADRDA + CERAD + NIA-Reagan or NFT count + Braak staging + amyloid plaque count	MMSE > 25	Not specified
29378	NINCDS-ADRDA + Braak staging + amyloid plaque count	Normal cognitive and functional examination	Not specified
36980	CERAD + Braak staging	No dementia	Not specified
84422	CERAD + Braak staging	Not specified	Not specified
48350	CERAD + NIA-Reagan + Braak staging	Cognitively and neurologically normal	DLB, PD, Binswanger's disease, MS, intracerebral hemorrhage

C)

Demographics of human samples						
	Control	EOAD	Control	LOAD	Control	MS
Age (median)	46	61	83	83	Unknown	Unknown
Sample size	10	4	63	59	5	5
Sex (% of females)	50	75	38	47	100	100